Master's Theses   Graduate School

Spring 2018

An Aerial Perspective: Using Unmanned Aerial Systems to Predict Presence of Lesser Earless Lizards (Holbrookia Maculata)

Sean Rogers
Fort Hays State University, scrogers3@mail.fhsu.edu

Follow this and additional works at: https://scholars.fhsu.edu/theses

Part of the Biology Commons

Recommended Citation

Rogers, Sean, "An Aerial Perspective: Using Unmanned Aerial Systems to Predict Presence of Lesser Earless Lizards (Holbrookia Maculata)" (2018). *Master's Theses*. 592.
https://scholars.fhsu.edu/theses/592

This Thesis is brought to you for free and open access by the Graduate School at FHSU Scholars Repository. It has been accepted for inclusion in Master's Theses by an authorized administrator of FHSU Scholars Repository.

AN AERIAL PERSPECTIVE: USING UNMANNED AERIAL SYSTEMS TO PREDICT

PRESENCE OF LESSER EARLESS LIZARDS (*HOLBROOKIA MACULATA*)

being

A Thesis Presented to the Graduate Faculty

of the Fort Hays State University in

Partial Fulfillment of the Requirements for

the Degree of Master of Science

by

Sean Rogers

B.S., Florida Southern College

Date_____   Approved_____
                                                          Major Professor

                                 Approved_____
                                                          Chair, Graduate Council

This thesis for

The Master of Science Degree

By

Sean Rogers

has been approved by

_____
Chair, Supervisory Committee

_____
Supervisory Committee

_____
Supervisory Committee

_____
Supervisory Committee

_____
Chair, Department of Biological
Sciences

ABSTRACT

Implementation of unmanned aerial system (UAS) in conservation biology has allowed researchers to extend their surveying range for monitoring wildlife. Wildlife biologists have started using UAS technology for detecting large species (i.e. elk, manatees) within their surveying range and monitoring changes and disturbance in the landscape. Despite this technological advancement, there are few studies that target smaller species (reptiles, rodents, amphibians) for UAS surveys. The primary reason for this is that these organisms are simply too small for detection for aerial surveying. However, certain species are restricted in their range because they have specific environmental requirements, and the target for UAS survey could change focus from detection of species to detection of their habitat. The Lesser Earless lizard (*Holbrookia maculata*) is smaller species of lizard that inhabits arid, rocky regions in the southwest United States, which is known to occupy areas of sparse vegetation and rocky or loamy soils. Although this species would be difficult to detect in aerial surveys, their habitat can easily be distinguished in aerial imagery. For this project, aerial surveys performed by UAS technology and ground surveying of *H. maculata* were analyzed in combination to generate a predictive model of *H. maculata* presence within a landscape. Three survey areas were assigned for this project: one to generate the predictive model from data collected from ground and aerial surveys, and two were assigned to assess the accuracy of the predictive model based off ground and aerial surveys.

RESUMEN

Aplicación de sistema aéreo no tripulado (UAS) en biología de la conservación ha permitido a los investigadores ampliar su gama de topografía para monitoreo de vida silvestre. Los biólogos de vida silvestre de la UAS han empezado a utilizar la tecnología para detectar las especies grandes (es decir, Elk, manatíes) dentro de su rango de topografía y seguimiento de los cambios y la perturbación en el paisaje. A pesar de este avance tecnológico, existen pocos estudios que target especies más pequeñas (reptiles, roedores, anfibios) de la UAS de encuestas. La razón principal de esto es que estos organismos son simplemente demasiado pequeña para detección de levantamientos aéreos. Sin embargo, algunas especies están restringidos en su rango porque tienen requisitos ambientales específicos, y la meta para la UAS encuesta podría cambiar el foco de la detección de especies para la detección de su hábitat. La menor (lagarto Earless Holbrookia maculata) es menor especie de lagartija que habita las zonas áridas, las regiones rocosas en el suroeste de Estados Unidos, que se sabe que ocupan áreas de escasa vegetación y rocas o suelos fértiles. Aunque esta especie sería difícil detectar en reconocimientos aéreos, su hábitat, pueden ser fácilmente distinguidos en imágenes aéreas. Para este proyecto, reconocimientos aéreos realizados por UAS tecnología y suelo topografía de H. maculata fueron analizados en combinación para generar un modelo predictivo de H. maculata presencia dentro de un paisaje. Tres áreas de estudio fueron asignados para este proyecto: uno para generar el modelo predictivo a partir de los datos recopilados a partir de reconocimientos terrestres y aéreos, y dos fueron asignados a evaluar la precisión del modelo predictivo basado en reconocimientos terrestres y aéreos

ACKNOWLEDGMENTS

Biological Sciences, and the city of Hays, would not have been quite as meaningful and definitely not as fun.

Lastly, I would like to thank my family, starting with my parents, John Rogers and Carolyn Bogaert. Their continuous love and encouragement throughout my life has helped me get to where I am today. I would like to thank my siblings, Kevan, Rhiannon, and Alex, for always being there when I need them. And finally, I would like to thank my loving wife, Frida, who stayed by my side throughout my entire graduate career. I could always count on her to be there for both the good times and the bad. I couldn't have asked for a better life partner to be by my side, and for that I am truly grateful.

TABLE OF CONTENTS

LIST OF TABLES

LIST OF FIGURES

PREFACE

This thesis is written in the style of The Southwestern Naturalist. These methods were exempted by the Institutional Animal Care and Use Committee of Fort Hays State University (IACUC protocol #17-0012).

INTRODUCTION

One of the most substantive advancements in remote-sensing technology over the past decade has been the commercialization of unmanned aircraft systems (UAS). Unmanned aerial systems have transitioned from primarily military applications, to a variety of applications among civilian users in earth-sensing reconnaissance and scientific data collection (Watts et al., 2012).

There are many advantages of using UAS over similar types of technology. For instance, conservation researchers currently rely on satellite-based remote sensing for mapping and monitoring land use change (Broich et al., 2011). High-resolution data is often crucial to accurately detect and track land use change at the landscape level; less than 1,000 ha (Koh and Wich, 2012). These high-resolution images are expensive to access, and freely available low-resolution satellite images such as Quickbird or IKONOS are secondary alternatives (Koh and Wich, 2012). However, what these low-resolution images make up for in affordability, they lose in critical data quality and often fall short of the accuracy necessary for some assessments and analyses.

In addition, satellite imagery is not always available because satellites travel in fixed orbits and return intervals (Ozesmi and Bauer, 2002). Cloud coverage affects satellite imagery, by distorting spectral signatures reflected from vegetation (Koh and Wich, 2012). This phenomenon is pronounced in areas around the tropics. Unmanned aerial systems provide the potential for researchers to perform surveys under their own supervision, and on a consistent basis instead of being dependent on the schedule of satellite imagery.

1

Unmanned aerial systems can be time and cost-efficient, compared to ground surveys. Most current assessment and monitoring of biodiversity is achieved by ground surveys, which cannot only be time consuming and expensive, but can also be challenging in remote areas (Gardner et al., 2008). These high cost surveys are often not conducted at the frequency required for proper analysis and monitoring of population trends (Meijaard et al., 2012). In Sumatra, ground surveys of Sumatran orangutan (*Pongo abelii*) populations can cost up to $250,000 for a two-year survey cycle (Koh and Wich, 2012). However, researchers were able to successfully perform UAS surveys of *P. albelii* with high accuracy at a fraction of the cost (Koh and Wich, 2012).

Another advantage of UAS technology is the ability to survey remote areas that have never been surveyed, due to difficult and inaccessible terrain. For example, NASA introduced the Sensor Integrated Environmental Remote Research Aircraft (SIERRA) in 2009, and has performed several missions that included measuring sea-ice roughness via remote sensing above the Arctic Circle, greenhouse gas monitoring in Railroad Valley, Nevada, mapping paths for groundwater flow in inaccessible terrain in Oregon and California, and hyperspectral bio-optical observations of seagrass around Cedar Key, Florida, and Buccal Reef, Tabago (Watts et al., 2012)

Wildlife researchers have begun to use UAS technology to survey alligators (*Alligator mississippiensis*), manatees (*Trichechus manatus*), dugongs (*Dugong dugon*), and black bears (*Ursus americansus*) (Chabot, 2009; Martin et al., 2012; Hodgson et al., 2013; Elsey and Trosclair, 2016). Prior to using UAS, wildlife researchers limited to manned aircraft as an aerial tool for monitoring wildlife (Patterson, 2015). The reasons for the shift to UAS technology is

that manned aircraft are expensive and can be dangerous for the pilot and passengers (Wiegmann and Taneja, 2003). In fact, aircraft crashes are one of the largest causes of mortality among field biologists (Sasse, 2003). Unmanned aerial systems offer a safer alternative for wildlife researchers that can perform the same tasks as manned aircraft. Manned aircraft are also known to disturb wildlife, which can negatively impact monitoring methods (Watts et al., 2010).

However, the small size of most UAS impose limitations on flight time and payload capacity relative to manned aircraft, especially when using a multi-rotor aircraft. The multi-rotor aircraft do not require a takeoff or landing runway like a fixed-wing aircraft and can fly at various altitudes. However, the multi-rotor UAS has high power requirements for flight, which reduces the total flight time of these models (Watts et al., 2012). Fixed-wing models can sustain flight for longer periods of time compared to the multi-rotor model, but require more room for takeoffs and landing, and do not have the ability to hover over areas of interest.

Most investigations using UAS for monitoring biodiversity are focused on larger animals (i.e., alligators, dugongs, etc.) but a few projects have targeted smaller species. Small animals are more difficult to detect in UAS derived imagery due to their small frame and cryptic behavior. For example, Watts et al. (2010) attempted to survey shorebirds using UAS technology in Florida, specifically targeting the endangered red knot (*Calidris canutus*). They were unable to accurately identify smaller shorebird species, but were successful in identifying larger species such as egrets (*Ardea alba, Bubulcus ibis,* and *Egretta* spp.), pelicans (*Pelecansu* spp.), and wood storks (*Mycteria americana*) (Watts et al., 2010). To be able to accurately identify smaller animals in UAS imagery, low altitude flights would be necessary, reducing the overall efficiency of data gathering and increase the amount of data to be processed. Flying at lower altitudes

3

requires more photos to be captured, because each image would capture a smaller, centralized image of the survey area.

Even though detecting smaller animals with UAS is challenging, specific habitat types can easily be detected by UAS aerial imagery. Rodriguez et al. (2012) conducted a project that incorporated ground survey data, with UAS data to analyze habitat selection of the Lesser Kestrel (*Falco naumanni*). Kabada (2014) analyzed habitat selection of Desert Kit Fox (*Vulpes macrotis arsipus*) by analyzing aerial imagery of burrows and surrounding vegetation. However, researchers have yet to use quantitative data, or airborne imaging spectroscopy (AIS), derived from UAS imagery in association with habitat selection. When analyzing different vegetation types, studies have shown that there is quantitative spectral difference among species (Gates et al., 1965; Gausman, 1985; Gong et al., 1997; Yu et al., 1999; Datt, 2000). Yu et al. (1999) analyzed the spectral reflectance patterns among several coniferous species in Sierra Nevada, California, and were accurate (76%) in being able to classify each species of conifer.

The reflectance signatures used to characterize vegetation are typically the red (~670 nm), green (~510 nm) blue (~470 nm), and near-infrared (~710 nm) wavelengths because plants use light in the visible light spectrum for photosynthetic activity and reflect the near-infrared (Rabideau et al., 1946; Gates et al., 1965; Loomis, 1965; Woolley, 1971; Gausman and Allen, 1973; Terashima et al., 2009). Previous studies have had success estimating vegetation diversity using spectral reflectance (Rochhini, 2007) as well as in modeling vegetation distributions (Pottier et al., 2014) using spectral data acquired from satellite imagery. Using higher resolution images available from UAS imagery could be a useful tool in predicting species presence based on spectral signatures of specific habitat types.

Lizard species that have strict microhabitat requirements are ideal models for testing the utility of UAS in characterizing these habitats in a large landscape. Reasons being that species that are habitat specialists are only found in certain areas within the landscape. The Lesser Earless Lizard (*Holbrookia maculata*) is a small phrynosomatid lizard that lives in the southwestern portion of the United States and inhabits areas associated with sparse, short vegetation, loose soil, and relatively level terrain (Degenhardt et al., 1996; Hammerson, 1999). In Nebraska, the abundance of these lizards is positively correlated with soil disturbance and cattle grazing (Ballinger and Jones, 1985; Ballinger and Watts, 1995). Another study reported that *H. maculata* were positively correlated with the areas of reduced vegetation created by prairie dogs (*Cynomys* spp.) (Davis and Theimer, 2003). In Kansas, populations *H. maculata* have been in decline (Platt, 1985), and recent surveys were unable to detect *H. maculata* in areas where they were formerly abundant (Taggart, pers. comm.).

My objectives were to determine if UAS technology could be used to identify spectral signatures that identify micro-habitat suitable for *H. maculata*, and use those spectral signatures to predict presence in a similar environment. In addition, I will use aero photographic imagery, imagery captured by manned aircraft, to determine whether differences in resolution affect predictive capabilities. I will also address the potential for UAS in conservation applications.

METHODS

Project Design

My study was designed to collect data to construct logistic regression models that could be used to predict presence of the Lesser Earless Lizard. Within the Hadley Ranch study site, I identified three survey plots: one plot, training plot, (~1.46 km^2) was used to generate a logistic

regression model based on the survey occurrences of *H. maculata* and remotely-sensed reflectance imagery. The remaining tests plots (~0.73 km^2) were used to test the accuracy of the logistic regression model. The survey plots were assigned based on whether the areas had appropriate habitat for *H. maculata*. The variables I used to predict occurrence of *H. maculata* were wavelength reflectances. These values were exported from the orthomosaics generated from both the UAS based imagery and aerophotographic-based imagery available from NAIP (National Agriculture Imagery Program) (Kansas Geological Survey, Kansas, USA). The herpetofaunal survey generated dichotomous data, presence and absence points; which meets requirements of a logistic regression.

Study Area

Hadley Ranch is a 12.9 km^2 prairie located in northeast Ellis County, Kansas. The local land use is primarily fossil fuel production and cattle grazing. The landscape is described as a semi-arid prairie ecoregion. Warm season mixed grasses are the dominate vegetation and interspersed with patches of sparse vegetation or exposed white chalky limestone rock at the surface. Within the study area there is an obvious upland to mesic lowland gradient. The xeric upland bluffs (~648 m above ground) (U.S. Department of Agriculture/Natural Resources Conservation Service, 2016) support a flora comprised of Little Blue-Stem (*Schizachyrium scoparium*), Smooth Sumac (*Rhus glabra*), Silver Sage (*Artemisia ludoviciana*), Yucca (*Yucca glauca*), Maximilian Sunflower (*Helianthus maximilliani*), Slim-Leaf Scurf-Pea (*Pediomelum linearifolium*), Resinous Skullcap (*Scutellaria resinosa*), Missouri Evening Primrose (*Oenothera macrocarpa*), and other species.

Near the center of the study site, the elevation drops precipitously (~631 m above ground) to a spring-fed water course. There are a few small ponds that are located in these areas, surrounded by cool season grasses. The common cool season grasses are Western Wheatgrass (*Pascopyrum smithii*) and Cheatgrass (*Bromus tectorum*), interspersed with patches of Feral Cannabis (*Cannabis sativa*), Ironweed (*Vernonia fasciculate*), and Western Ragweed (*Ambrosia psilostachya*).

Ground Survey

I conducted ground surveys to identify *H. maculata* from May through September of 2017. Three survey plots were assigned within the landscape. One plot (~1.46 km^2) was used to generate a species presence model based on both ground and aerial data. The other two plots (~0.73 km^2/each) were used to test the accuracy of the model. I performed ground surveys to identify and georeference the presence of individuals with Garmin® Oregon 550t in habitat space. Searches were timed to calculate catch-per unit effort (CPUE) within each plot. Although I did not designate transects, GPS track logs were used as a reference to highlight areas that were previously surveyed, to ensure all habitat types were thoroughly examined with minimal bias. At least two researchers were present to survey each day of sampling. I performed surveys between 1000 and 1600 Central Time Zone (CTZ). The target species for this project, *H. maculata,* was chosen based on relative abundance in the area, the uncertainty of its conservation status, and its apparent narrow habitat selection. *Holbrookia maculata* occupy areas of sparse vegetation that would be easier to identify and characterize from a UAS imagery and characterized. Other common lizard species at the site include Texas Horned Lizard (*Phrynosoma cornutum*), Six-lined Racerunner (*Aspidoscelis sexlineata*), and the Prairie Lizard (*Sceloporus consobrinus*).

Phrynosoma cornutum and *A. sexlineata* occupy very similar habitats to *H. maculata*, but *S. consobrinus* is expected in areas of denser vegetation.

Unmanned Aerial Systems Survey

The UAS vehicle I used for this project was an Altimapper, a custom built fixed-wing model (Aerovision, South Africa) with a 2 m wingspan. The UAS was designed with a built-in sensor compartment that allowed for efficient image capture. The batteries for the UAS were lithium ion batteries (10.5 Ah, 22.2 v, 360 w) and capable of supporting 75 minutes of flight times. The sensor I used for this project was Sony Alpha 5100 camera with a modified filter to allow detection of near-infrared (~710 nm), green (~510 nm), and blue (~470 nm) wavelengths of reflectance at image resolutions as fine as 2 cm/pixel or ground sampling distance (GSD).

All of my flights were conducted between 1000 and 1400 CTZ to capture the optimum light reflectance and minimize the effects of shadows. A Pixhawk® autopilot (Computer Vision and Geometry Lab, Zurich, Switzerland) was used to control flight characteristics of the aircraft. The software interface I used to design and execute flights was Mission Planner (Ardupilot: Oborne, 2010). The images were tiled together to construct an orthomosaic of the study area. An orthomosaic is a compilation of aerial images constructed from overlapping images and adjusted for perspective and scale (Hawkins, 2016). I used Agisoft PhotoScan (Agisoft LLC, St. Petersburg, Russia) to generate the orthomosaics. The program detects keypoints in the aerial imagery and generates a descriptor for each point. The descriptors are then used to detect correspondences across all photos. (Semyonov, pers. comm.). Generally, the more keypoints shared among images the higher degree of visual accuracy in the orthomosaics.

To ensure spatial accuracy of the orthomosaic, I placed ground control points (GCPs) in each survey area. Ground control points are unique markers planted in each survey plot with a known location. These markers were a 0.6 m x 0.6 m piece of corrugated plastic that were uniquely patterned to be easily identified in the aerial imagery. I georeferenced the GCPs by marking their locations with the Garmin® Oregon 550t and captured in the aerial images during flights. When creating an orthomosaic of the study area, these GCPs provide regional accuracy of where the orthomosaic was positioned on the earth. This is an important detail of the project, especially when transferring the orthomosaic data to other programs (ArcGIS) for data analysis.

Training plot. I flew a modified Sony α 5100 sensor which was flown 120 m above ground level (AGL) and at 16 m/s to capture 1,594 images having a ground resolution of 2.56 cm/pixel (Figure 1). The total flight time was ~1 hour 10 minutes to survey the 1.6 km^2 plot. I used all images to generate the orthomosaics of the training plot. The flight was performed in July, 2017.

Testing plots. Using the same sensors and aircraft, I flew the West and South plots (Figures 3 and 4) at 120 m AGL and 16m/s to capture 1,307 images having a ground resolution of 2.29 cm/pixel. The total flight area was 2.17 km^2 and total flight time of the UAS was ~1 hour and 15 minutes. I used all images to generate the orthomosaics of both West and South survey plots. The flight was also performed in July, 2017

Aerophotographic Imagery

Aerophotographic imagery was incorporated to compare the utility of UAS imagery to predict species presence. The aerial imagery was provided by the United State Department of Agriculture (USDA) by the National Agriculture Imagery Program (NAIP). The NAIP file was

captured in 2015, during the growing seasons to create orthophotography available for private

and public use. This could affect our comparisons between data sets. However, the 2015 was

used in the analysis because it was the most recent data file available, and it is similar to other

imagery that would be available to wildlife biologists for conservation planning. The imagery

captured by NAIP for Kansas includes broad width red, green, and blue wavelengths at GSD of 1

m. The 2015 NAIP imagery was exported from the Kansas Data Access & Support Center

(DASC) (Kansas Geological Survey, Kansas, USA).

Statistical Analysis

I used a logistic regression analysis to determine if the presence of *H. maculata* could be

predicted from reflectance values. My georeferenced observations of *H. maculata* were imported

into ArcGIS 10.5 (ESRI Geographic Information Systems, California, USA) along with the

orthomosaics generated by Agisoft Photoscan (Agisoft LLC, St. Petersburg, Russia). I generated

pseudo-absence points from a random distribution within our training survey plot. Reflectance

values of near-infrared (NIR; ~780nm), blue (~470 nm), and green light (~510 nm) were

extracted at each presence and pseudo-absence point from the orthomosaics. Those values were

used as predictor variables for the logistic regression model. Reflectance values from the same

locations were extracted from the NAIP imagery. However, red light (~670 nm) reflectance

values were extracted instead of near-infrared because the NAIP imagery contained only red,

blue, and green reflectance values. Each data sets was then used to construct a logistic regression

model using R (R Core Team, Vienna, Austria) based on light reflectance values extracted from

both data sets. After the models were constructed, the UAS orthomosaics were transformed

based on the logit transformation, to generate probability maps to assess prediction accuracy of

10

the UAS predictive model. Probability values predicted to be 0.50 or greater were determined to predict presence and vice-versa.

I generated a classification matrix to describe the performance of both UAS and NAIP generated logistic regression models. The classification matrix compares the predicted presences and absences with the actual presence and pseudo-absence values generated from the logistic regression models.

I used a Mann-Whitney analyisis (R) to test difference between presence and pseudo-absence mean probability values within the 2 test plots (West and South), extracted from the transformed orthomosaics. The reasoning for this test was to determine if predicted probability values where *H. maculata* are present were statistically different from predicted probability values of pseudo-absences. Pseudo-absence points were generated in both South and West survey (tests) plots from random points by using ArcGIS. I generated a 5-meter buffer at each point, and the zonal statistics tool was used to extract probability values. The 5-meter buffer was generated around each point in an attempt to reduce sampling error and compensate for sporadic movements of the lizards. The maximum probability in each buffer was used to perform the Mann-Whitney test. Insights should provide with the types of areas *H. maculata* are likely to occur based on blue light reflectance.

RESULTS

Ground Survey

From May to September of 2017, a total of 128 *H. maculata* observations were recorded (Table 1). The majority of observations of *H. maculata* were in areas of sparse vegetation in

11

exposed gravelly soil between patches of *S. scoparium* and *S. resinosa*. The total number of person-hours surveying all 3 areas was approximately 380 hours.

The total number of person-hours surveyed in the training plot was approximately 114 hours and resulted in 65 observations of *H. maculata* (Figure 2). The catch per unit effort (CPUE) of *H. maculata* in the training plot was 0.566 per person-hr (Table 2).

In the West plot, the total number of person-hours surveying was 106 hours and resulted in 33 observations of *H. maculata* (Figure 3). The CPUE of *H. maculata* in the west plot was 0.311 per person-hr.

In the South plot, the total number of person-hours surveying was 160 hours and resulted 35 observations *H. maculata* (Figure 4). The CPUE of *H. maculata* in the South plot was 0.219 per person-hr (Table 2).

Logistic Regression

Prior to performing the logistic regression models, I examined both data sets with a scatterplot matrix that illustrates comparisons between each variable (Figures 7 and 8). When analyzing the co-linearity of variables, the green and blue wavelengths were strongly correlated, which I took into consideration when executing the logistic regression (Figure 7). Other relationships observed in the data set include a few outliers present in the NIR data set, as well as the right skewed distribution of the green variable data (Figure 7). In the NAIP imagery data set, all 3 bands (RGB) were seen to be multi co-linear (Figure 8). However, there appeared to be no issue of normality among the variables, and no outliers were present in the data (Figure 8).

The results of the first logistic regression model generated with the UAS data, indicated that NIR and blue reflectance may predict the occurrence of *H. maculata* (df = 126, t = 2.576, p

= 0.0111) (Blue: df = 126, t = 4.629, p < 0.001; NIR: df = 126, t = -3.799, p < 0.001) (Table 3) It should also be noted that the first logistic regression models generated with UAS reflectance data ran into problems with underdispersion (0.363). This suggests that the model is conservative (increased Type II errors). Accordingly, I used a quasi-binomial distribution model for these data to address the low dispersion, which explains the reasoning for t-score values being presented.

I generated a second model by using only NIR and blue wavelength reflectance to analyze the two significant predictor variables of the first model. The second model was statistically significant as well (df = 127, t = 3.205, p = 0.00171); (Blue: df =127, t = 5.402, p < 0.001; NIR: df = 127, t = -5.184, p < 0.001). However, the relationship between NIR reflectance values and presence of *H. maculata* appeared to be complex, as the presence points were distributed evenly among the NIR reflectance values (Figure 5). Therefore, I dismissed NIR from the model.

Finally, by using only blue wavelength reflectance, the model was also statistically significant (df = 128, t = 3.921, p < 0.001); (Blue: df = 128, t = 3.921, p < 0.001) (Table 3). An ANOVA indicated a significant difference (F = 34.583, df = 126, p < 0.001) between the reduced model (Blue) and the full model (NIR, Green, and Blue); (Table 6).

I generated a classification matrix to analyze the accuracy of the reduced logistic regression model (Table 4). When determining presence, the model had a true positive rate of 1. The misclassification rate of the model was 0.0461. The false positive rate was 0.092, and the specificity (correct to predicting absence) was 0.908. The precision of the classification matrix was 0.916. I performed a X^2 test to analyze the classification matrix, which suggests that the predictive model is valid (X^2 = 108.22, df = 3, p < 0.0001); (Table 5).

13

The first logistic regression model I generated based on NAIP derived reflectance incorporated all 3 bands (RGB) was significant and predicted presence of Lesser Earless Lizard (df = 126, z = 3.995, p < 0.001; Blue: df = 126, z = 4.29, p < 0.001; NIR: df = 126, z = -1.657, p = 0.0974; Green: df = 126, z = -0.75, p = 0.4532). The blue light reflectance had the most effect on the model (df = 126, z = 4.29, p < 0.001), so I generated a reduced model for the blue wavelength values. The reduced model was significant and predicted presence of Lesser Earless Lizard (df = 129, z = 6.247, p < 0.001). The dispersion of the reduced model was closer to 1 (0.76197), so there was not a problem with over or under dispersion of the dependent variable, and the binomial dispersion model was used. I performed an ANOVA to assess differences between the full and reduced model. As with the UAS analysis, the test detected differences between both models (F = -13.366, df = 126, p < 0.001) (Table 10).

I generated a classification matrix to analyze the accuracy of the reduced model from the NAIP imagery (Table 8). The true positive rate was lower in comparison to the UAS model (0.8548), and had a higher false positive rate (0.1384). Both the precision (0.8548) and the specificity (0.8615) were lower than the UAS model, suggesting that the UAS data generated a more accurate predictive model compared to the NAIP imagery (Table 11). I performed a X^2 test to analyze the classification matrix, which suggests that the NAIP model is also valid (X^2 = 59.846, df = 3, p < 0.0001) (Table 9).

I transformed the orthomosaics in ArcGIS 10.5 using the raster calculator, to generate probability maps based on the logit transformation. The only variable that was included with the regression coefficient was blue light reflectance because, it was the only variable that was statistically significant (Figures 9 and 10).

14

The cutoff value for predicting presence was p = 0.50; any pixel with a probability value of 0.50 or higher was a predicted presence. After I converted the orthomosaics from West and South plots (test plots) to probability of presence, I imported occurrence points of *H. maculata* into ArcGIS. Around each presence point, I generated a 5-meter buffer to compensate for variation in the movement of each individual and variation in location error of the GPS unit (Figures 11 and 12). I used the zonal statistics tool in ArcGIS to extract all values within each buffer generated around each point of presence. For this project, I used the maximum probability value to determine accuracy of the logistic regression model.

I used maximum values instead of means, because the mean reflectance values would not truly represent the habitat in which *H. maculata* were observed. For example, if an individual was marked near the edge of a blowout area, an exposed patch of rocky or sandy substrate with little to no vegetation, the buffer zone generated around the presence point could contain more pixels in the denser vegetation than in the blowout or sparse vegetation areas. The mean probability values would then be lower than expected relative of where the individual was located. For the West survey plot, 31 out of the 33 (0.939) presence marks were determined to predict presence of *H. maculata*, and for the South survey plot, 34 out of 35 (0.971) presence marks were also determined to predict presence. Based on the model generated from the training plot data and actual presence data in both survey (test) plots, the model appears to have high predictive power (65/68; = 0.956). I performed a Mann-Whitney test to evaluate the difference in mean probability values (blue light) among presence and absence points of *H. maculata*. The reason the Mann-Whitney was performed was to examine the relationship between blue light reflectance and presence or absence *H. maculata*. For both test plots, there was statistically significant difference between maximum

probability of presence and absence points (West: W = 71.5, n = 66, p < 0.001; South: W = 133.5, n = 70, p < 0.001) (Tables 12 and 13; Figures 13 and 14). This suggests that the occurrence of *H. maculata* is not randomly distributed among the landscape.

DISCUSSION

The majority of observations for *H. maculata* were in areas with sparse vegetation, and rocky or gravelly soil. This is consistent with habitat descriptions for *H. maculata* and their natural history (Ballinger et al., 1979; Ballinger and Jones, 1985; Rosenblum, 2008). Because these areas characteristically have little to no vegetation, they can be readily detected in satellite and UAS aerial imagery. It is possible to quantify habitat by using the reflectance values in the orthomosaic generated from aerial imagery. Because habitat used by *H. maculata* is sparsely vegetated, the reflectance of solar radiation is high in these areas (Gates et al., 1965; Gausman and Allen, 1973; Loomis, 1965; Rabideau et al., 1946; Woolley, 1971). This explains the relationship (Figure 6) between presence and high values of reflected blue light. When analyzing near-infrared reflectance (710 nm) (Figure 5), there is no discernable pattern because live vegetation reflects electromagnetic radiation greater than 700 nm (Gates et al., 1965; Gausman and Allen, 1973; Loomis, 1965; Rabideau et al., 1946; Woolley, 1971). Areas with rocky substrate and dense vegetation both reflect near-infrared light and consequently there is no relationship with the presence of *H. maculata*.

Plants reflect green light (~510 nm) relative to other colors of the visible light spectrum (Terashima et al., 2009). The reason there is a strong association to blue light reflectance and *H. maculata* presence, is that plants most readily absorb light in the blue light spectrum (470 nm), and the red light spectrum (670 nm) (Gates et al., 1965; Gausman and Allen, 1973; Loomis,

1965; Rabideau et al., 1946; Terashima et al., 2009;Woolley, 1971). Because the sensor was modified to capture images in the near-infrared, green, and blue region, instead of a typical camera that captures images in RBG spectrum, there is no analysis of what the red light spectrum (670 nm) might have in this project. Despite not having red light reflectance data in this project, blue light still provides clear insight into the usefulness of aerial imagery.

When analyzing the orthomosaics in the blue light reflectance, there was a substantial amount of variation within the landscape (Figure 16). Densely vegetated areas reflect less blue light, and surfaces like roads and gravel reflect more blue light, which creates heterogeneity in the orthomosaic that can be used to interpret patterns in the landscape. When analyzing orthomosaics in the near-infrared or green reflectance, the features in the vegetation do not appear as prominent in the landscape and are arguably more homogenous across the entire study area (Figures 17 and 18). Therefore, I observed less variation in wavelength reflectance in the near-infrared and green light spectrum in the orthomosaics.

Based off the rates between the UAS and NAIP classification matrices, the UAS logistic regression model appears to have more predictive power compared to the NAIP logistic regression model (Table 11). Higher resolution in UAS imagery (< 5cm/pixel) seemed to enhance the predictive model, in comparison to the lower resolution images captured by aerophotography (1 m/pixel). These high resolution images generated a more detailed orthomosaic, containing precise data of the landscape. Because of this, the UAS predictive model had a lower misclassification rate (~5%) compared to NAIP model (~16%). It was evident when looking at the results of the two test plots (West, South). I was able to have relatively high predicting accuracy using the generated predictive model with UAS data (~94%, ~97%).

The spatial scale of a study will determine whether the effort to generate an orthomosaic from sUAS imagery or other aerial imagery is more appropriate. Based on the sUAS and the orthomosaics, it seemed appropriate for my project and projects of slightly greater extent. When comparing other platforms for acquiring remote sense data, such as satellite or manned aircraft, UAS are effective in areas in the range of 1-10 km^2 (Dandois and Ellis, 2013; Whitehead et al., 2014). This is supported when comparing the overall effectiveness between the UAS data and the aerophotographic data, because UAS data generated a more accurate predictive model (Table 11). The GSD of UAS data (< 5 cm) compared to the aerophotography data (~1 m) provided more detailed and contemporaneous assessment of the landscape. However, using a UAS platform to capture imagery of this quality in areas larger than 10 km^2 would need to be considered carefully, because the computer processing power necessary to assemble the orthomosaics would be beyond available desktop microcomputers capabilities. In addition, sUAS flight times would be longer, which might increase variation in the imagery due to shadows and changes in the angle of the incidence of solar radiation.

Location of *H.* maculata might have been altered because of the sampling protocol. Encounters with *H. maculata* were the result of walking in the landscape. The actual detection of lizards typically occurred when the individuals were retreating. Lizards might have moved from other habitats and were unable to be seen until they were in areas that were easier to see movement (e.g. blowout areas with little vegetation).

Visual inspection of orthomosaics indicated artifacts in the imagery. Streaks of dark pixels as seen in some areas of the orthomosaics, which could be the result of several factors. These dark areas could be due to insufficient overlap of the UAS survey. During construction of

the orthomosaics, the software (Agisoft Photoscan) that aligns the images by identifying pixel values in separate images. If several images contain the same pixel value, the software will generate a tie point, which provides the software a reference for aligning the images. If an area is not surveyed thoroughly, the software cannot detect sufficient tie points and images can be misalign.

The sensor might have shifted during flight, which can inhibit the sensor's ability to capture images. During the flight, the lens angle might have shifted and captured images with the shadow of the platform. A dark semi-circle appeared in the top left corner of some the images. This could affect the ability of Agisoft Photoscan to align images and therefore create artifacts in the orthomosaics.

 The duration of the surveys were just over an hour. During that time, changes in environmental conditions could affect image quality (cloud cover; wind gust; changes in wind direction). I considered cloud coverage for each flight to minimize shadows (shadow effect) in the images. Shadow effects might alter the images due to different lighting. This could result in lower number of tie points. Also, shadow effects reduce reflectance accuracy because images are the result of different lighting.

Wind gusts can unpredictably alter the course of the UAS platform during flight. Each aerial survey performed by the UAS is programmed into the autopilot, which directs the UAS where to fly, the speed, and altitude of the platform. Even with onboard GPS to guide aerial surveys, strong winds might alter the flight path and speed of the UAS, which can either cause the UAS to capture images in the wrong pathways or capture too few images if the UAS is forced to fly faster than the intended speed.

While *H. maculata* are not a species of conservation concern in the United States, this technique could be useful for assessing habitats of threatened or endangered species. For instance the Texas Horned Lizard (*P. cornutum*) is comparable to *H. maculata* and occupies similar habitat and has similar ecological requirements. In Texas, *P. cornutum* is a threatened species due primarily to habitat loss from urbanization, and the introduction of fire ants (*Solenopsis invicta*). The use of UAS systems could provide more timely and cost effective habitat monitoring to aide in conservation efforts in these organisms.

Increases in anthropogenic disturbance associated with agriculture, fossil fuels extraction, and urbanization, will increase pressure for conservationists and agency professionals to monitor land use (Sieg et al., 1999). Performing surveys with UAS systems will allow land managers to quickly survey the land and the possible presence of threatened or endangered species, i.e. *P. cornutum*. This could allow for conservationists to focus time and effort in areas that are more suitable to these species, and use limited resources most efficiently. Using UAS systems for surveying or monitoring potential habitat and should be considered for landscape and conservation planning.

Literature Cited

BALLINGER, R. E., J. D. LYNCH, AND P.H. COLE. 1979. Distribution and natural history of
amphibians and reptiles in western Nebraska with ecological notes on the herpetiles of
Arapaho Prairie. Prairie Naturalist 11:65-74

BALLINGER, R. E., AND S. M. JONES. 1985. Ecological disturbance in a sandhills prairie:
impact and importance to the lizard community on Arapaho Prairie in western Nebraska.
Prairie Naturalist 17.

BALLINGER, R. E., AND K. S. WATTS. 1995. Path to Extinction: Impact of Vegetational
Change on Lizard Populations on Arapaho Prairie in the Nebraska Sandhills. The
American Midland Naturalist 134:413–417

BROICH, M, M. C. HANSEN, P. POTAPOV, B. ADUSEI, E. LINDQUIST, AND S. V.
STEHMAN. 2011. Time-series analysis of multi-resolution optical imagery for
quantifying forest cover loss in Sumatra and Kalimantan, Indonesia. International Journal
of Applied Earth Observation and Geoinformation 13:277-291.

CHABOT. D. 2009. Systematic evaluation of a stock unmanned aerial vehicle (UAV) system for
small-scale wildlife survey applications. Ph.D dissertation, McGill University, Montreal
Quebec.

DANDOIS J. P., AND E. C. ELLIS. 2013. High spatial resolution three-dimensional mapping of
vegetation spectral dynamics using computer vision. Remote Sensing of
Environment 136:259-276.

DATT, B. 2000. Identification of green and dry vegetation components with a cross-correlogram
spectral matching technique. International Journal of Remote Sensing 21:2133-2139.

DAVIS, J. R., AND T. C. THEIMER. 2003. Increased lesser earless lizard (Holbrookia

   maculata) abundance on Gunnison's prairie dog colonies and short term responses to

   artificial prairie dog burrows. The American Midland Naturalist 150:282-290.

DEGENHARDT, W. G., C. W. PAINTER, AND A. H. PRICE. 1996. Amphibians and reptiles

   of New Mexico. University of New Mexico Press, Albuquerque, New Mexico. 19

ELSEY, R. M., AND P. L. TROSCLAIR III. 2016. The usse of an unmanned aerial vehicle to

   locate alligator nests. Southeastern Naturalist.

GARDNER, TOBY A., J. BARLOW, T.C. AVILA-pIRES , A. B. BONALDO, J. E. COSTA, M.

   C. ESPOSITO, L. V. FERREIRA, J. HAWES, M. L. HERNANDEZ, M. S.

   HOOGMOED, R. N. LEITE, N. F. LO-MAN-HUNG, J.R. MALCOLM, M. B.

   MARTINS, L. A. MESTRE, R. MIRANDA-SANTOS, W. L.OVERAL, L. PARRY, S.

   L. PETERS, M. A. RIBEIRO-JUNIOR, M. N. DA SILVA, C. DA SILVA MOTTA,

   AND C. A. PERES. 2008. The cost-effectiveness of biodiversity surveys in tropical

   forests. Ecology letters 11:139-150.

GATES, DAVID M., H. J. KEEGAN, J. C. SCHLETER, AND V. R. WEIDNER, 1965. Spectral

   properties of plants. Applied Optics 4:11-20.

GAUSMAN, H. W. 1985. Plant leaf optical properties in visible and near-infrared light. Applied

   Optics 24:3305

GAUSMAN, H. W., AND W. A. ALLEN. 1973. Optical parameters of leaves of 30 plant

   species. Plant Physiology 52:57-62.

GONG, P., R. PU, AND B. YU. 1997. Conifer species recognition: An exploratory analysis of in

   situ hyperspectral data. Remote sensing of Environment 62:189-200.

HAMMERSON, G. A. 1999. Amphibians and reptiles in Colorado. University Press of
Colorado. Boulder, Colorado.

HAWKINS, S. 2016. Using a drone and photogrammetry software to create orthomosaic images
and 3D models of aircraft accident sites. ISASI 2016 Seminar:1-26

HODGSON, A., K. NATALIE, AND D. PEEL. 2013. Unmanned aerial vehicles (UAVs) for
surveying marine fauna: a dugong case study. PloS One 8: e79556. Retrieved from
https://doi.org/10.1371/journal.pone.0079556

KADABA, D. 2014. Ecology of the desert kit fox (Vulpes macrotis arsipus) in Chuckwalla
Valley, California. M.S. thesis, Duke University, Durham, North Carolina

KOH, L. P., AND S. A. WICH. 2012. Dawn of drone ecology: low-cost autonomous aerial
vehicles for conservation. Tropical Conservation Science 5:121-132.

LOOMIS, W. E. 1965. Absorption of radiant energy by leaves. Ecolog*y* 46: 14-17.

MARTIN J., H. H. EDWARDS, M. A. BURGESS, H.F. PERCIVAL, AND D.E. FAGAN.
2012. Estimating Distribution of Hidden Objects with Drones: From Tennis Balls to
Manatees. PLoS ONE 7: e38882. doi:10.1371/journal.pone.0038882

MEIJAARD, E., S.WICH, M. ANCRENAZ, AND A. J. MARSHALL, 2012. Not by science
alone: why orangutan conservationists must think outside the box. Annals of the New
York Academy Science 1249:29-44.

OBORNE, M. 2010. MissionPlanner (1.3.48) [Computer software]. Retrieved from
http://ardupilot.org/planner/docs/common-install-mission-planner.html

OZESMI, S. L., AND M. E. BAUER. 2002. Satellite remote sensing of wetlands. Wetlands
Ecology and Management 10:381-402.

PATTERSON, C. 2015. Evaluation of an unmanned aircraft system for detecting. Ph.D dissertation. McGill University, Montreal, Quebec, Canada.

PLATT, D. R., 1985. Population trends and habitat assessment of snakes and lizards in south central Kansas. Final report. Kansas Fish and Game Commission, Pratt, Kansas. Contract 80:1-36

POTTIER, J., Z. MALENOVSKÝ, A. PSOMAS, L. HOMOLOVÁ, M. E. SCHAEPMAN, P. CHOLER, AND N. E. ZIMMERMANN. 2014. Modelling plant species distribution in alpine grasslands using airborne imaging spectroscopy. Biology letters, 10:20140347. doi:10.1098%2Frsbl.2014.0347

RABIDEAU, G. S., C. S. FRENCH, AND A. S. HOLT. 1946. The absorption and reflection spectra of leaves, chloroplast suspensions, and chloroplast fragments as measured in an Ulbricht sphere. American Journal of Botany 33:769-777.

ROCCHINI, D., 2007. Effects of spatial and spectral resolution in estimating ecosystem α-diversity by satellite imagery. Remote sensing of Environment. 111:423-434.

RODRÍGUEZ, A., J.J. NEGRO, M. MULERO, C. RODRÍGUEZ, J. HERNÁNDEZ-PLIEGO, AND J. BUSTAMANTE. 2012. The Eye in the Sky: Combined Use of Unmanned Aerial Systems and GPS Data Loggers for Ecological Research and Conservation of Small Birds. PLoS ONE 7: e50336. Retrieved from https://doi.org/10.1371/journal.pone.0050336

ROSENBLUM, E. B. 2008. Preference for local mates in a recently diverged population of the lesser earless lizard (Holbrookia maculata) at White Sands. Journal of Herpetology 42:572-583.

SASSE, D. B. 2003. Job-related mortality of wildlife workers in the United States, 1937-
2000. Wildlife Society Bulletin 31:1015-1020.

SIEG, C. H., H. F. CURTIS, AND S. MCCANNY. 1999. Recent biodiversity patterns in the
Great Plains: implications for restoration and management. Great Plains Research 9:277-
313.

TERASHIMA, I., T. FUJITA, T. INOUE, W. S. CHOW, AND R. OGUCHI. 2009. Green light
drives leaf photosynthesis more efficiently than red light in strong white light: revisiting
the enigmatic question of why leaves are green. Plant and cell physiology. 50:684-697

U.S. Department of Agriculture/Natural Resources Conservation Service. *LiDAR 2016*.
Elevation Data. Lawrence, KS. Kansas Data Access and Support Center (2016)

WATTS, A. C., J. H. PERRY, S. E. SMITH, M. A. BURGESS, B. E. WILKINSON, Z.
SZANTOI, AND H. F. PERCIVAL. 2010. Small unmanned aircraft systems for low-
altitude aerial surveys. Journal of Wildlife Management. 74:1614-1619.

WATTS, A. C., V. G. AMBROSIA, AND E. A. HINKLEY. 2012. Unmanned aircraft systems in
remote sensing and scientific research: Classification and considerations of use. Remote
Sensing 4:1671-1692.

WIEGMANN, D. A., AND N. TANEJA. 2003. Analysis of injuries among pilots involved in
fatal general aviation airplane accidents. Accident Analysis & Prevention 35:571-577.

WHITEHEAD, K., AND C. H. HUGENHOLTZ. 2014. Remote sensing of the environment with
small unmanned aircraft systems (UASs), part 1: a review of progress and
challenges. Journal of Unmanned Vehicle Systems 2:69-85

WOOLLEY, J. T. 1971. Reflectance and transmittance of light by leaves. Plant

    physiology 47:656-662.

YU, B., M. OSTLAND, P. GONG, AND R. PU. 1999. Penalized discriminant analysis of in situ

    hyperspectral data for conifer species recognition. IEEE transactions on Geoscience and

    remote sensing, 37:2569-2577.

Table 1: Summary table of all *H. maculata* encountered during ground surveys at Hadley Ranch in all survey plots from May-September 2017.

	Training Plot	South Plot	West Plot
Lesser Earless Lizard (*Holbrookia maculata*)	65	35	33
n =	133		

Table 2: The catch per unit effort (CPUE) of each survey plot from May – September 2017 at Hadley Ranch. CPUE is the proportion of the total number of species observed by the number of total person-hours surveyed (person/hr).

	Training Plot	South Plot	West Plot
CPUE (Earless Lizard)	0.566 person/hr	0.219 person/hr	0.311 person/hr
CPUE (total species)	0.775 person/hr	0.525 person/hr	0.368 person/hr

Table 3: List of all the variables included to generate the logistic regression model from the UAS data, the descriptive statistics of that data, and the results of each logistic regression model generated. All reflectance values were extracted with ArcGIS at presence and pseudo-absence occurrences in the training plot. Analysis was performed in R software.

Variables	Variable Description
NIR	Near-infrared light reflectance values (780 nm)
Green	Green light reflectance values (510 nm)
Blue	Blue light reflectance values (470 nm)

	N	Minimum	Maximum	Mean	Std. Deviation
NIR	130	37	222	135.2923	38.60081
Green	130	23	169	69.66923	36.00891
Blue	130	19	214	113.4	56.90147

	Model 1		Model 2		Model 3	
Variable	Coefficient	t-stat	Coefficient	t-stat	Coefficient	t-stat
Constant	-7.89077	-2.546	-9.4757	-3.205	-8.89495	-3.605
Blue	0.30927	4.629	0.28252	5.402	0.07494	3.921
NIR	-0.31103	-3.799	-0.21251	-5.184		
Green	0.09596	1.753				
Degrees of Freedom	126		127		128	

29

Table 4: The classification matrix is the results of the most reduced logistic regression model (Model 3 in Table 3) from UAS data, and the calculated rates. Classification matrix was performed using R software. Misclassification rate is the how often is the model wrong (False predictions/Total size), True Positive Rate is when the model correctly predicts presence (Predicted Presence/Actual Presence), False Positive Rate is the when the model predicts absence when its actually presence (False Absence/Actual Absence), Specificity is when its actually absence, how often does the model predict absence (Predicted Absence/Actual Absence), Precision is when the model predicts presence and is correct (Predicted Presence/Actual Presence), and the Prevalence is how often does presence actually occur (Actual Presence/Total size).

n=130	Predicted Absence	Predicted Presence	
Actual Absence	59	6	65
Actual Presence	0	65	65
	59	71	

Misclassification Rate	0.046153846
True Positive Rate	1
False Positive Rate	0.092307692
Specificity	0.907692308
Precision	0.915492958
Prevalence	0.5

Table 5: Results of the Chi-squared test of independence performed in R software of the reduced UAS logistic regression model. Data is based on the classification matrix table generated in Table 4. This test determines whether or not there is a relationship between presence and absence variables.

X^2	df	p
108.22	3	< 0.0001

Table 6: Results of the ANOVA performed in R software, of the reduced UAS logistic regression model (blue only), to the full model (NIR, green, blue). This test determines whether or not the performance of the reduced model is comparable to the full model.

F	Df	p
34.583	126	< 0.0001

Table 7: List of all the variables included to generate the logistic regression model from the NAIP data, the descriptive statistics of that data, and the results of each logistic regression model generated. All reflectance values were extracted with ArcGIS at presence and pseudo-absence occurrences in the training plot. Analysis performed in R software

Variables	Variable Description
Red	Red light reflectance values (710 nm)
Green	Green light reflectance values (510 nm)
Blue	Blue light reflectance values (470 nm)

	N	Minimum	Maximum	Mean	Std. Deviation
Red	130	24	214	142.5462	44.56184
Green	130	33	216	143.4154	42.31099
Blue	130	37	202	122.8692	43.37426

	Model 1			Model 2	
Variable	Coefficient	F		Coefficient	F
Constant	-4.99357	3.995		-6.76136	6.247
Blue	0.16183	4.290		0.05588	6.277
Red	-0.06161	1.657			
Green	0.09596	1.753			
Degrees of Freedom	126			128	

Table 8: The classification matrix is the results of the most reduced logistic regression model (Model 2) from the NAIP data, and the calculated rates. Classification matrix was performed using R software. Misclassification rate is the how often is the model wrong (False predictions/Total size), True Positive Rate is when the model correctly predicts presence (Predicted Presence/Actual Presence), False Positive Rate is the when the model predicts absence when its actually presence (False Absence/Actual Absence), Specificity is when its actually absence, how often does the model predict absence (Predicted Absence/Actual Absence), Precision is when the model predicts presence and is correct (Predicted Presence/Actual Presence), and the Prevalence is how often does presence actually occur (Actual Presence/Total size).

n=130	Predicted Absence	Predicted Presence	
Actual Absence	56	9	65
Actual Presence	12	53	65
	68	62	

Misclassification Rate	0.161538461
True Positive Rate	0.854838709
False Positive Rate	0.138461538
Specificity	0.861538461
Precision	0.854838709
Prevalence	0.5

Table 9: Results of the Chi-squared test of independence performed in R software, of the reduced NAIP logistic regression model. Data is based on the classification matrix table generated in Table 8. This test determines whether or not there is a relationship between presence and absence variables.

X^2	df	p
59.846	3	< 0.0001

Table 10: Results of the ANOVA performed in R software, of the reduced NAIP logistic regression model (blue only), to the full model (NIR, green, blue). This test determines whether or not the performance of the reduced model is comparable to the full model.

F	Df	p
-13.366	126	0.001252

Table 11: Table compares the different rates of both classification matrices generated in Tables 4 and 8. Misclassification rate is the how often is the model wrong (False predictions/Total size), True Positive Rate is when the model correctly predicts presence (Predicted Presence/Actual Presence), False Positive Rate is the when the model predicts absence when its actually presence (False Absence/Actual Absence), Specificity is when its actually absence, how often does the model predict absence (Predicted Absence/Actual Absence), Precision is when the model predicts presence and is correct (Predicted Presence/Actual Presence), and the Prevalence is how often does presence actually occur (Actual Presence/Total size).

	UAS Imagery	NAIP Imagery
Misclassification Rate	0.046153846	0.161538461
True Positive Rate	1	0.854838709
False Positive Rate	0.092307692	0.138461538
Specificity	0.907692308	0.861538461
Precision	0.915492958	0.854838709
Prevalence	0.5	0.5

Table 12: Mann-Whitney test statistics to determine difference of probability values among presence (n = 35) and pseudo-absence (n = 35) buffers in the South plot. Probability values were extracted from the transformed orthomosaics using ArcGIS in Figure 10. The maximum reflectance value was extracted from each buffer.

Variable	N	Std. Deviation	Minimum	Maximum	Median
Present	35	16.537	17.6535	99.9633	99.7427
Absent	35	32.2537	8.0173	99.9964	47.1282

W		α		p-value	
133.5		0.05		1.564 e-08	

Table 13: Mann-Whitney test statistics to determine difference of probability values among presence ($n = 33$) and pseudo-absence ($n = 33$) buffers in the West plot. Probability values were extracted from the transformed orthomosaics using ArcGIS in Figure 9. The maximum reflectance value was extracted from each buffer.

Variable	N	Std. Deviation	Minimum	Maximum	Median
Present	33	10.59438	41.5809	99.9964	99.9163
Absent	33	25.13266	12.842	99.9964	54.6119

W		α		p-value	
71.5		0.05		6.753 e-10	

Figure 1: Map of the three survey plots (Training, West, and South plots) throughout the months of May-September of 2017, at the study site Hadley Ranch, located just north of Hays, Kasas, USA.
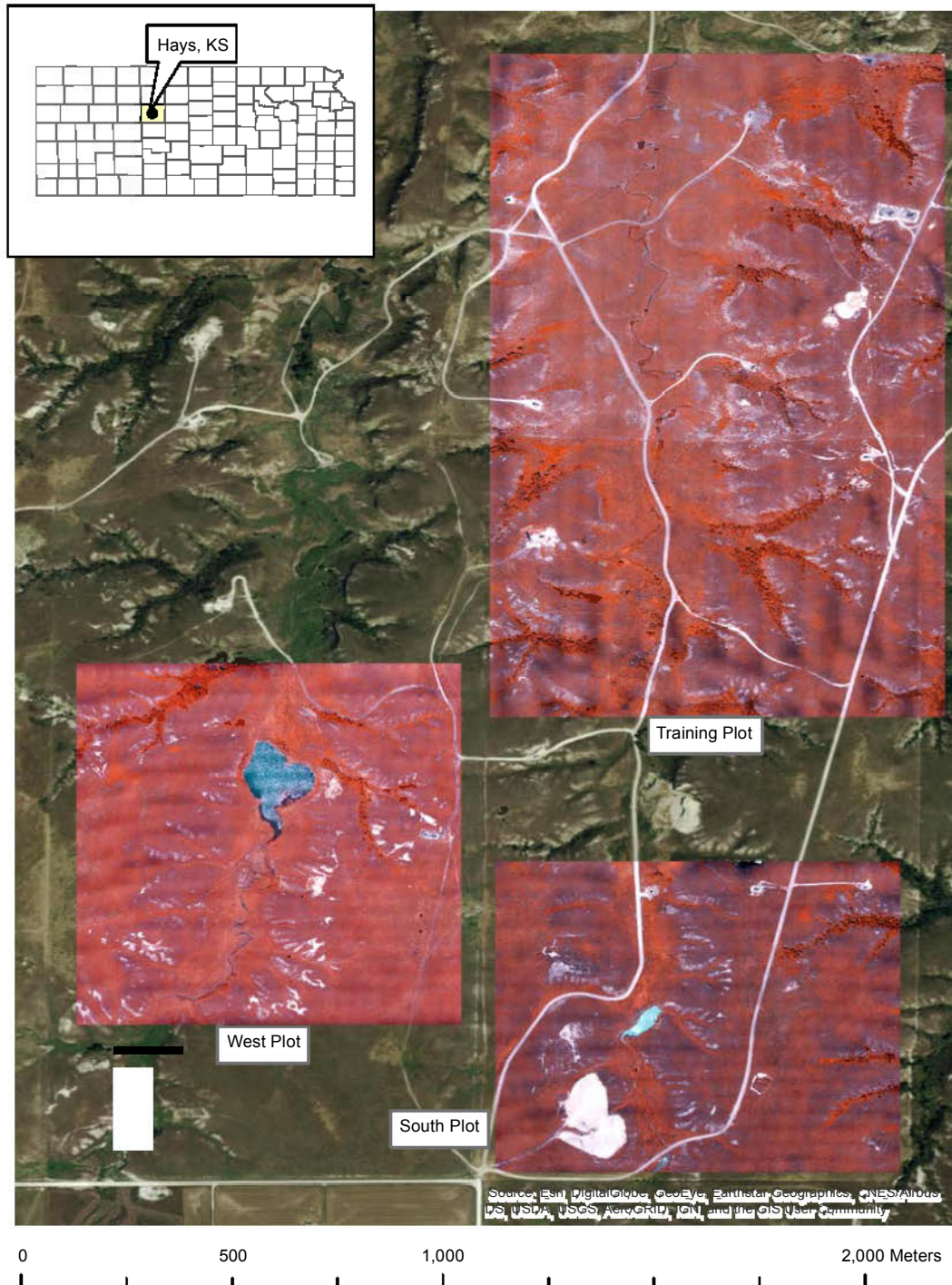
Figure 2. Map of all 65 *H. maculata* presence points in the Training Plot at Hadley Ranch, with 65 pseudo-random generated absence points. Surveys performed from May-September, 2017.
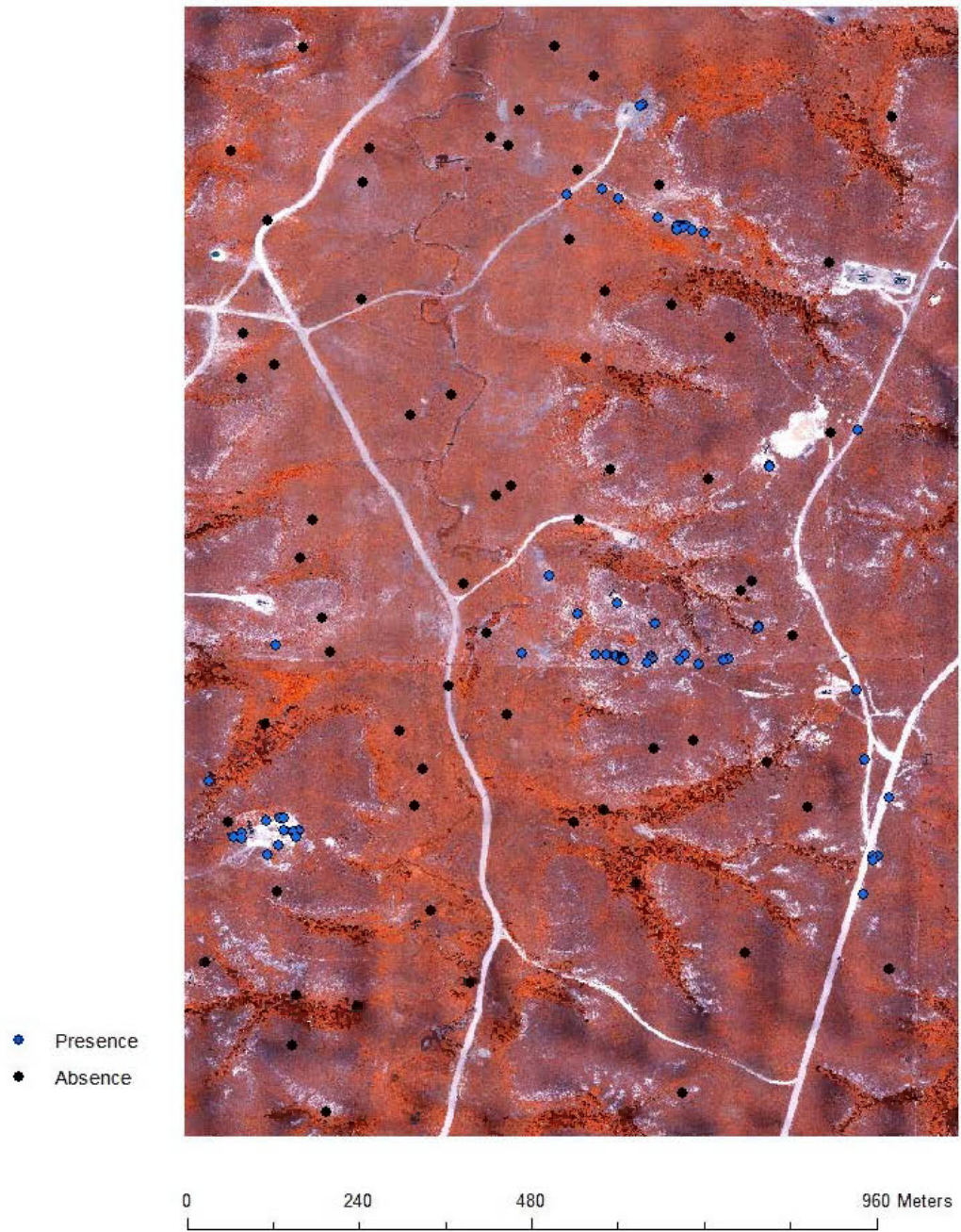
Figure 3: Map of all 33 *H. maculata* presence points observed in Hadley Ranch with a 5 meter buffer in the West Plot. Surveys performed from May-September, 2017.

Legend

Recorded Presence w/5m buffer

Figure 4: Map of all 35 *H. maculata* presence points observed in Hadley Ranch with a 5 meter buffer in the South Plot. Surveys performed from May-September, 2017.
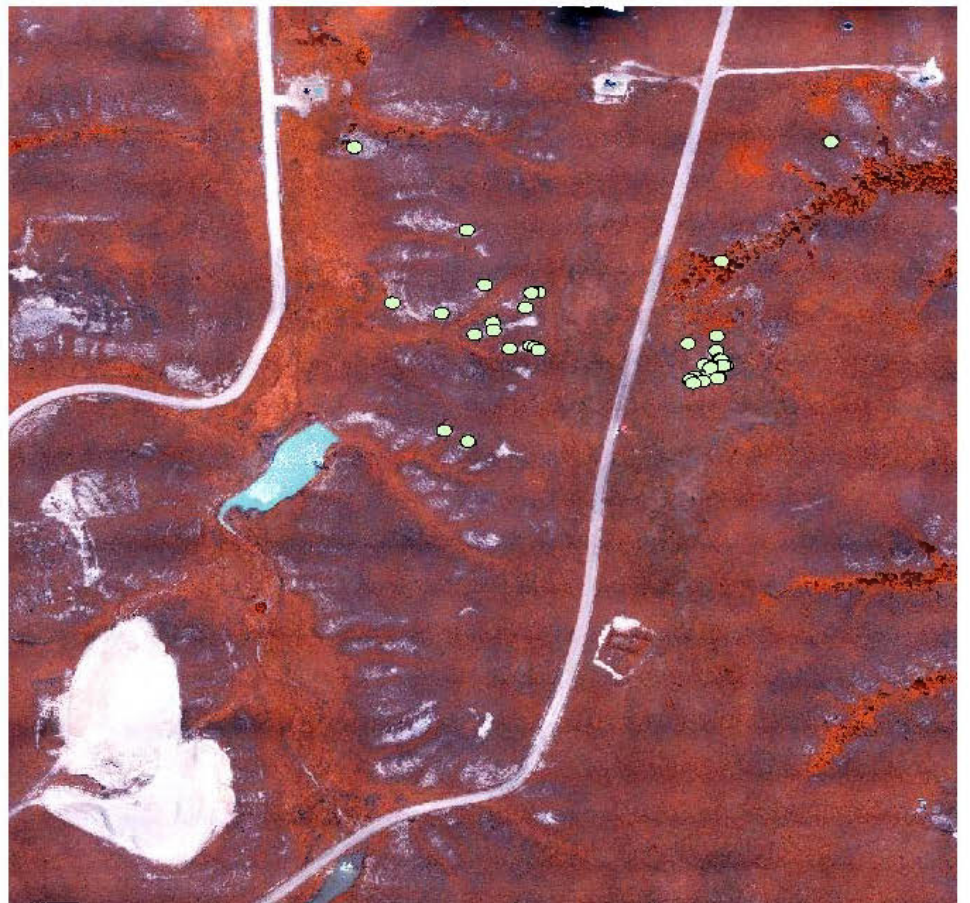
Legend

Recorded Presence w/5m buffer

Figure 5: Graph that describes the relationship between presence points and near infrared light (~710 nm) reflectance values from the UAS data. Points with a value of 1 are determined to predict presence and points with a value of 0 are determined to predict absences.
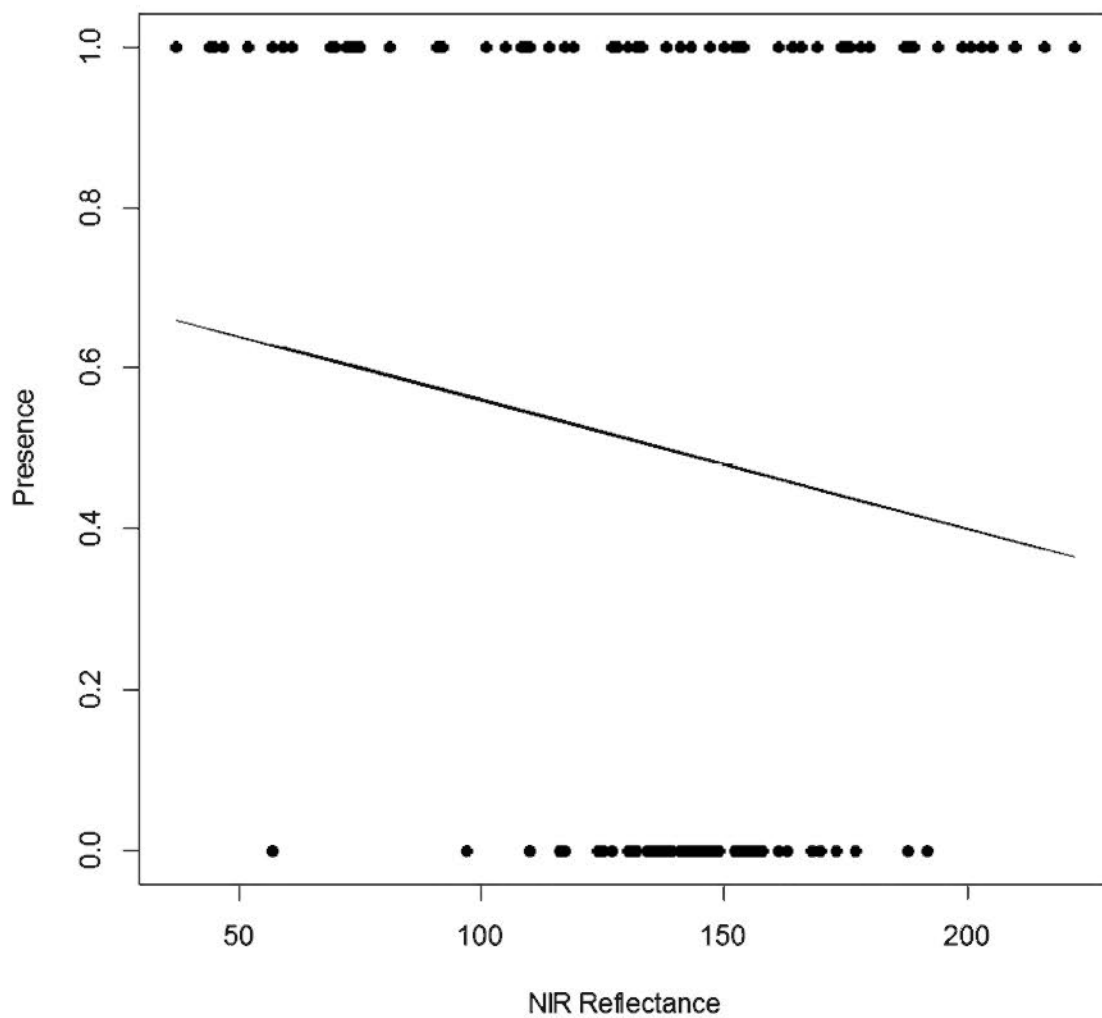
Figure 6: Graph that describes the relationship between presence points and blue light (~470 nm) reflectance values from the UAS data. Points with value of 1 are determined to predict presence and points with a value of 0 are determined to predict absences.
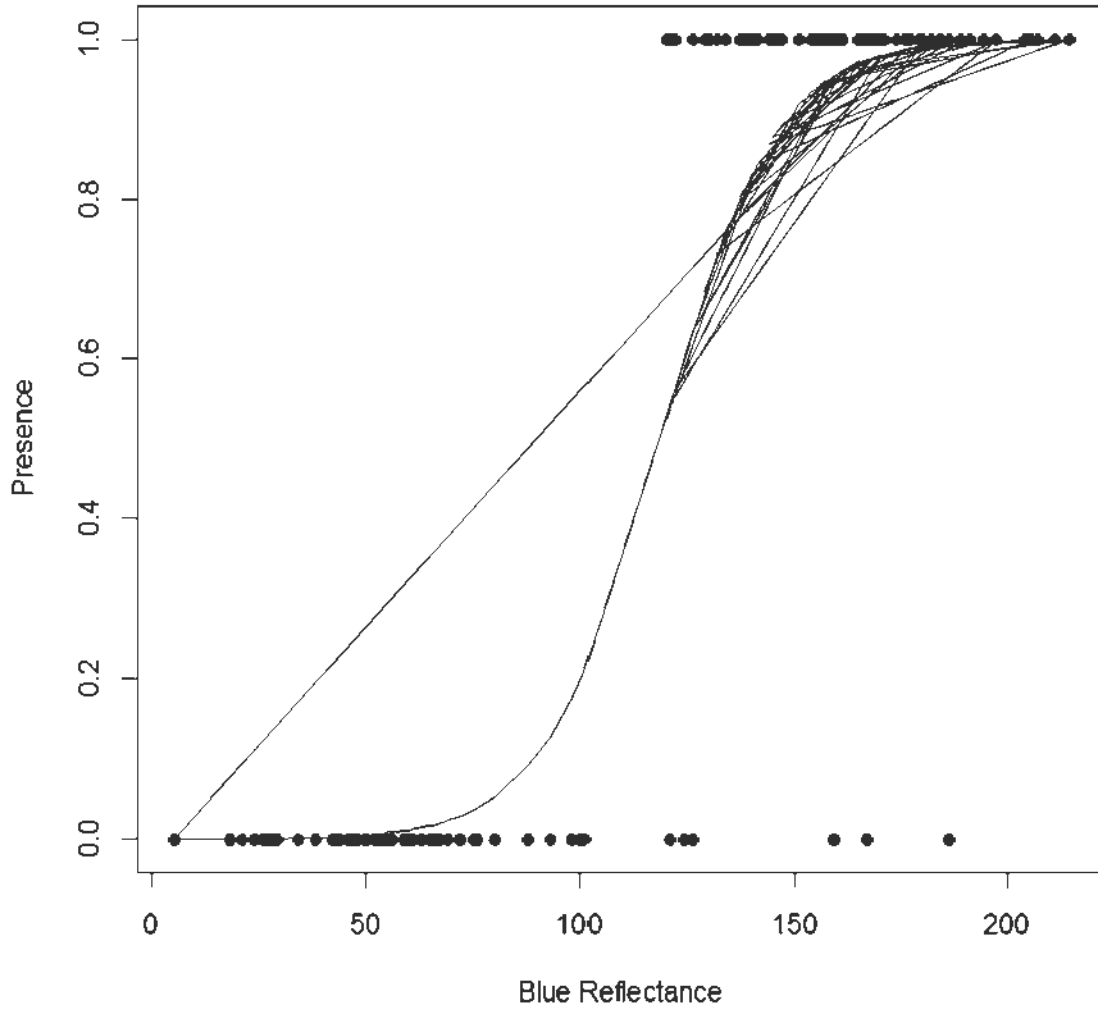
Figure 7: Scatterplot matrix that analyzes the relationships between all variables in the UAS data set. Boxes labeled Presence, NIR, Green, and Blue illustrate the presence/pseudo-absence data, and the other matrices compare each variable among each other to assess linear correlations.
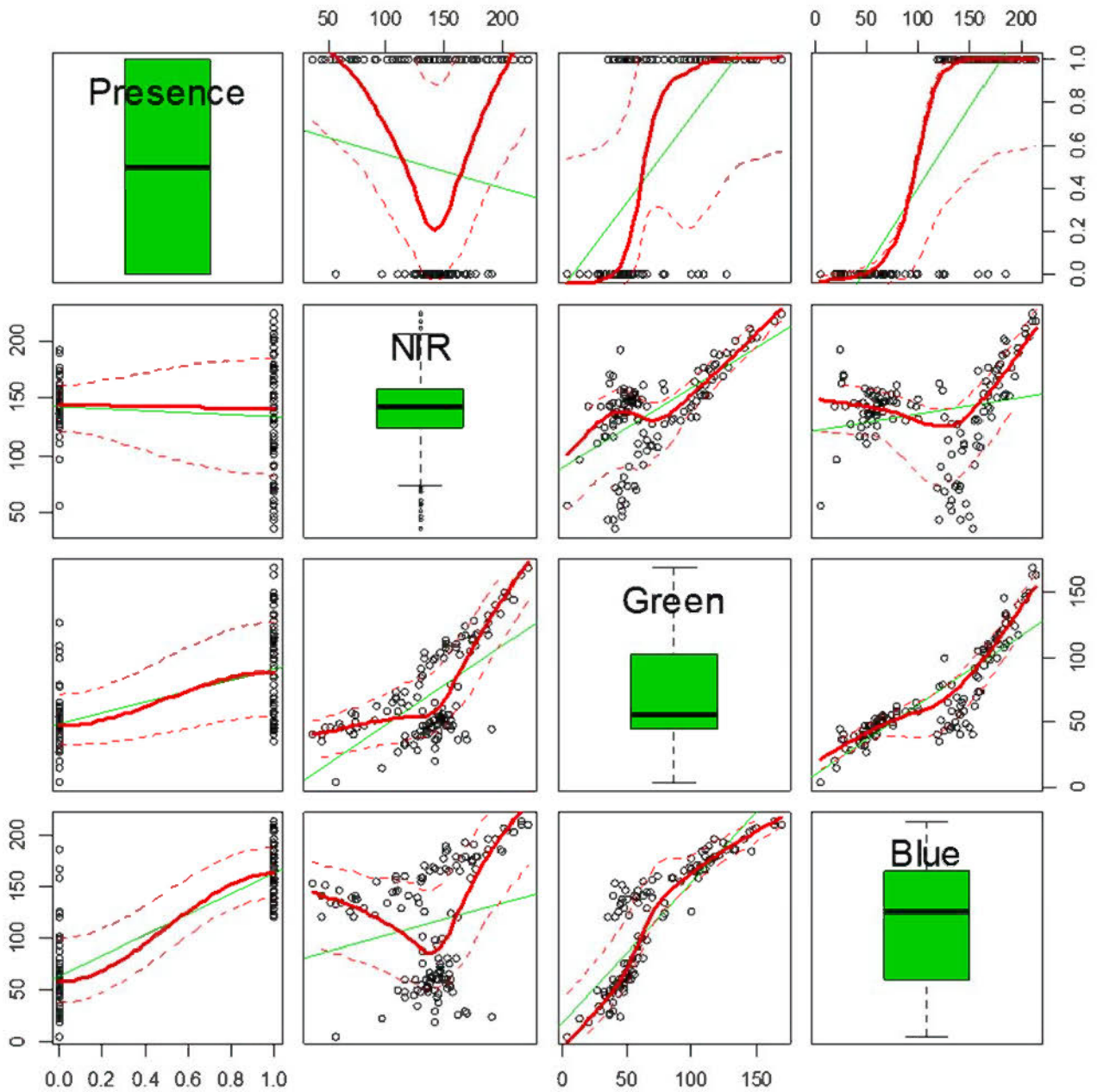
Figure 8: Scatterplot matrix that analyzes the relationships between all variables in the NAIP data set. Boxes labeled Presence, NIR, Green, and Blue illustrate the presence/pseudo-absence data, and the other matrices compare each variable among each other to assess linear correlations.
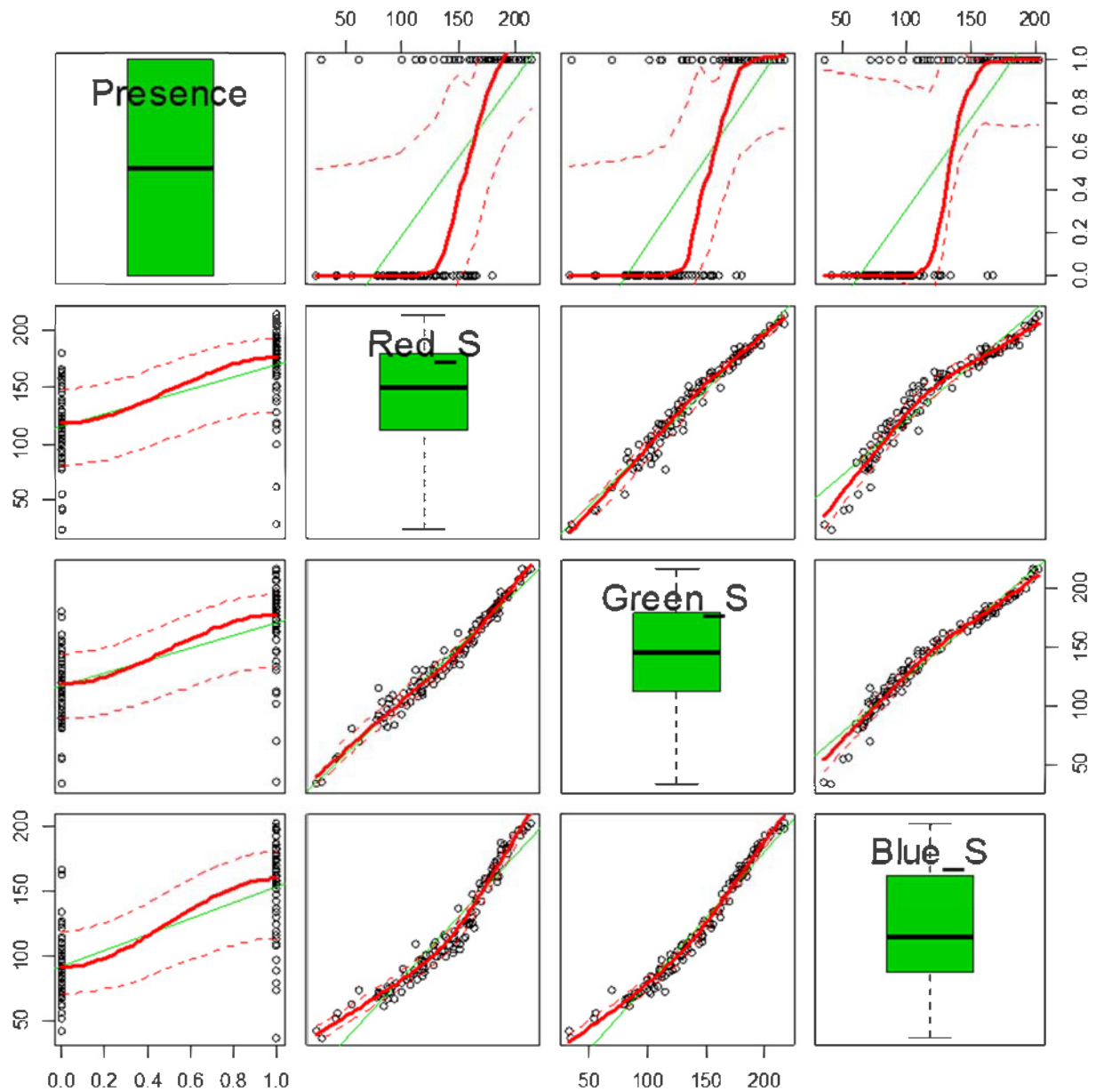
Figure 9: Graph that describes the relationship between presence points and blue light (~470 nm) reflectance values from the NAIP data. Points with a value of 1 are determined to predict presence and points with a value of 0 are determined to predict absences.
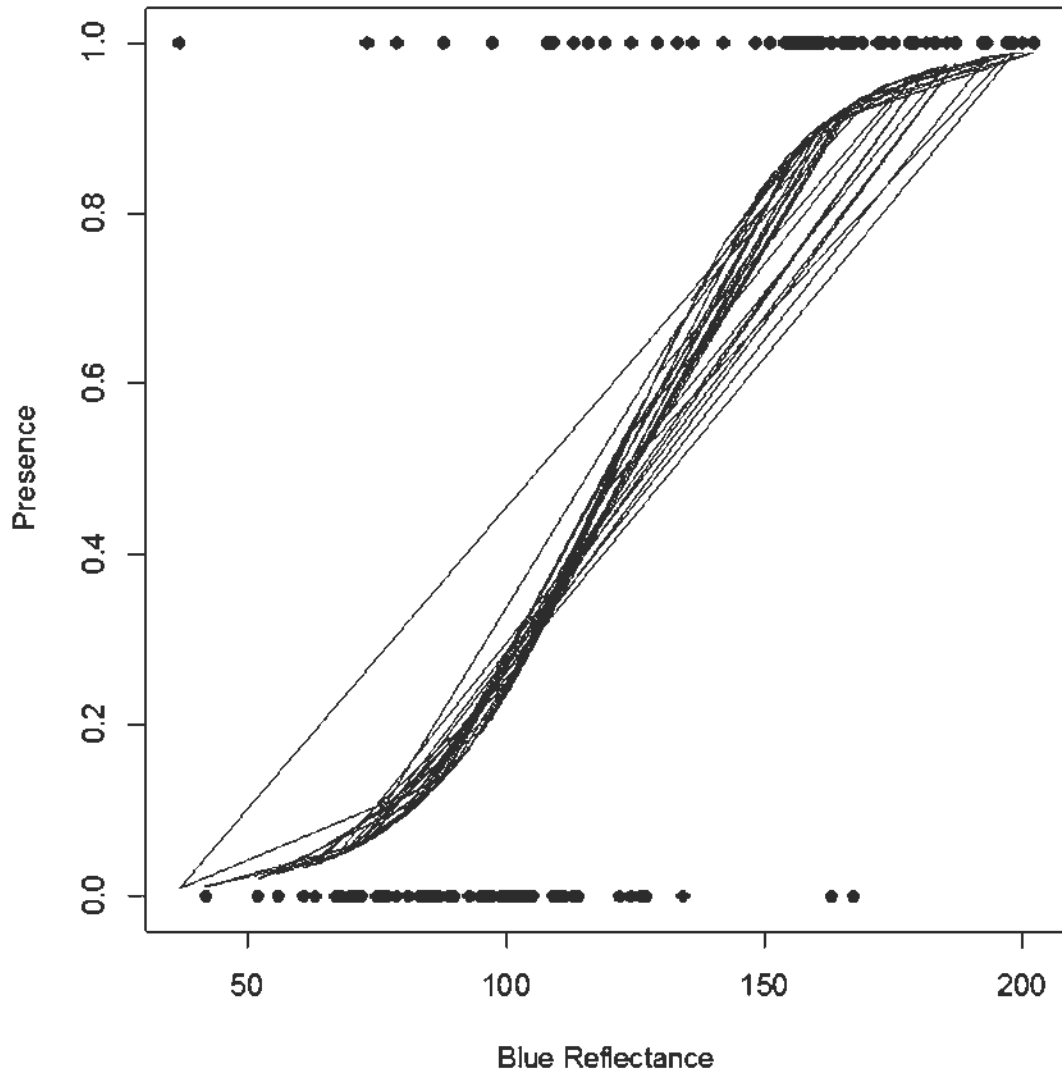
Figure 10: Map that represents presence probability values based on the logit transformation of blue light reflectance within the West Plot of Hadley Ranch. Image captured in July, 2017.
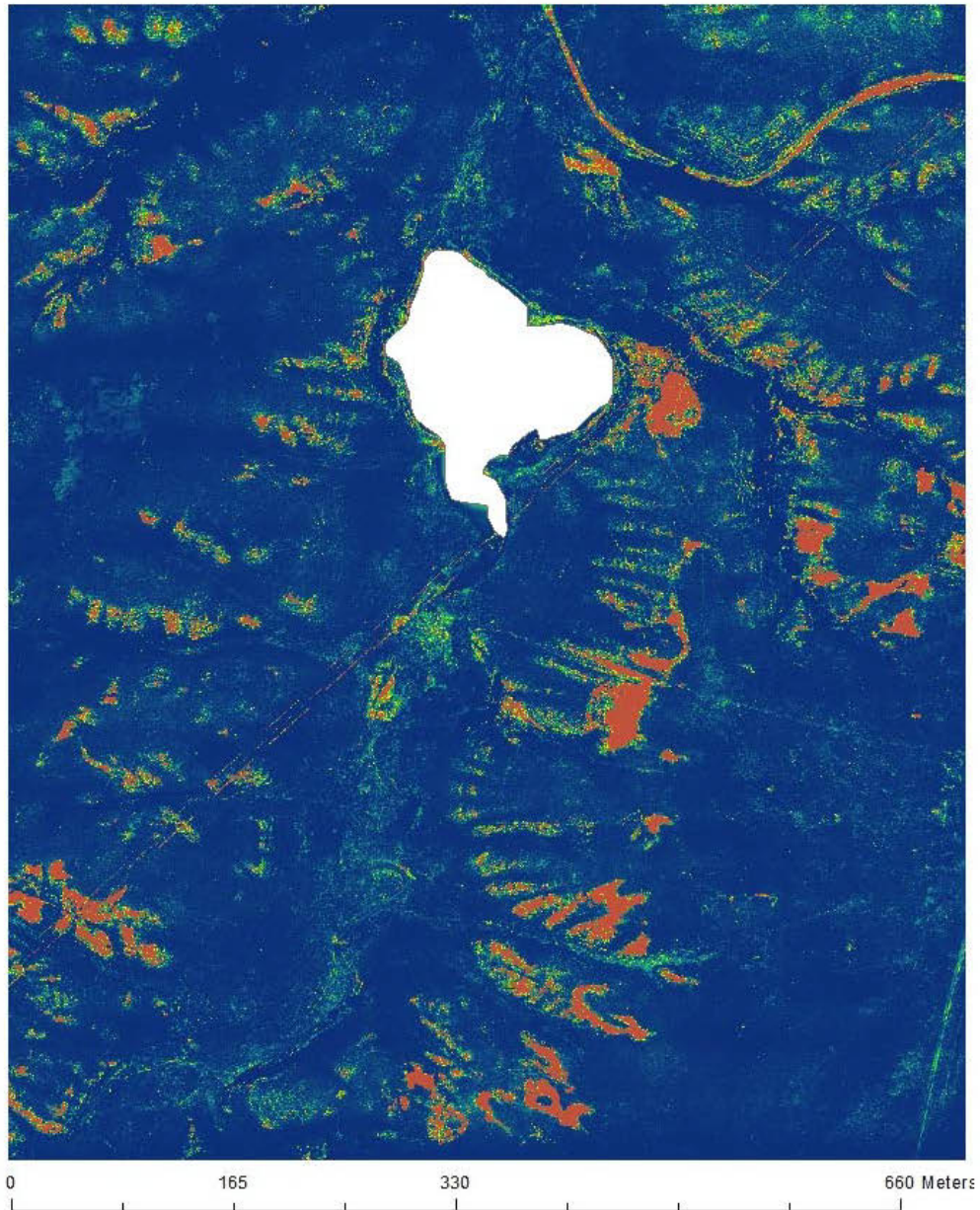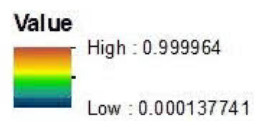
Figure 11: Map that represents presence probability values based on the logit transformation of blue light reflectance within the South Plot of Hadley Ranch. Image captured in July, 2017.
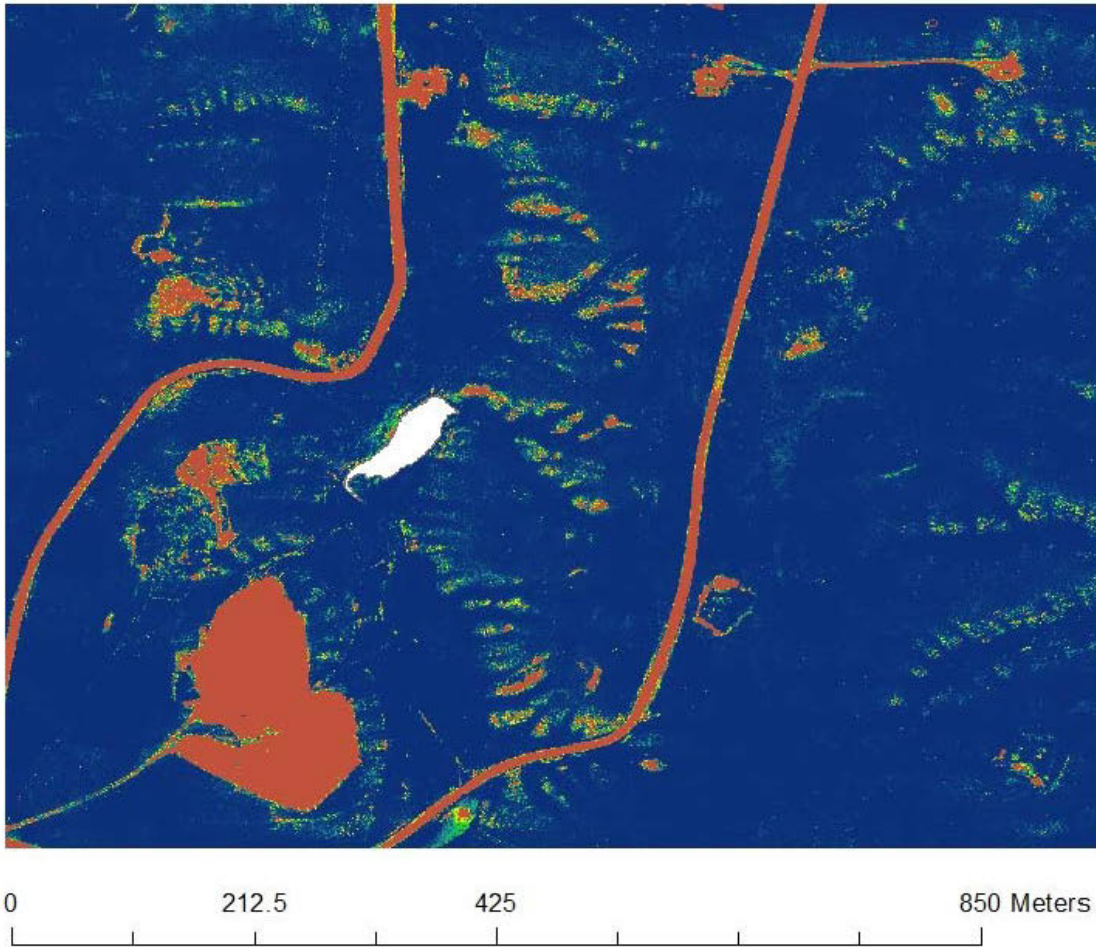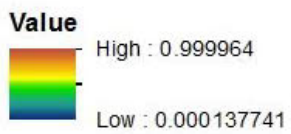
Figure 12: Map of all 33 *H. maculata* individuals with a generated 5 meter buffer and the presence probability of the West plot reclassified into two groups; predicted presence (p > 0.50) and predicted absence (p < 0.05).
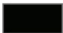
Figure 13: Map of all 35 *H. maculata* individuals with a generated 5 meter buffer and the presence probability of the South plot reclassified into two groups; predicted presence (p > 0.50) and predicted absence (p < 0.05).
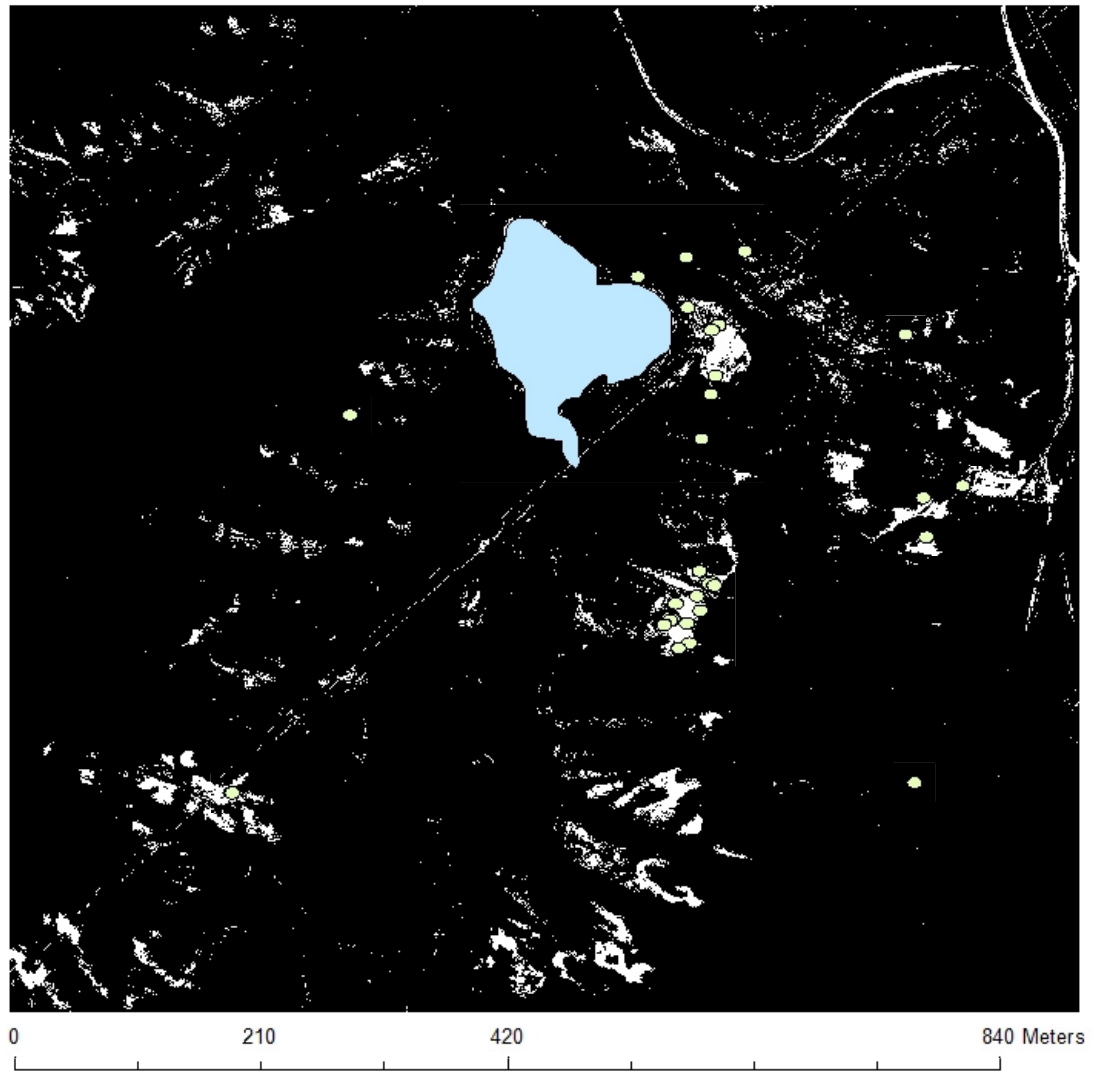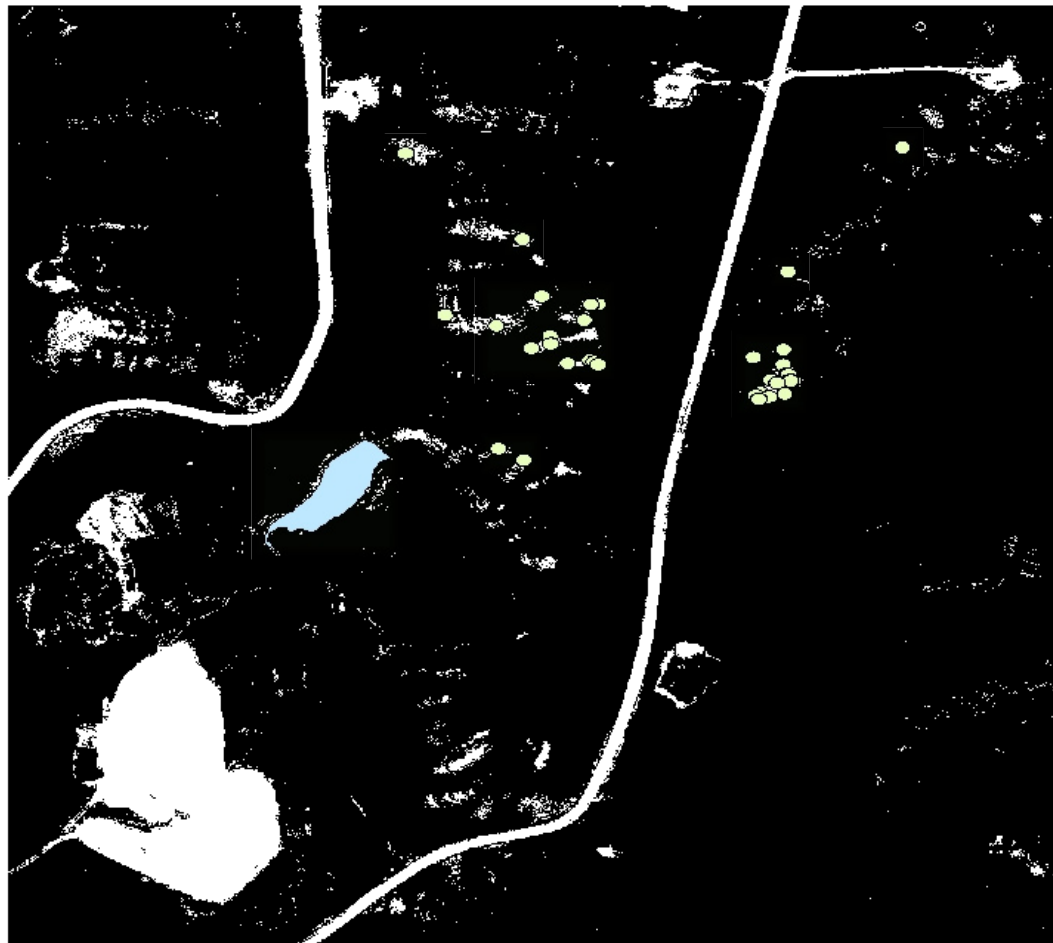
Legend
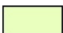
▢ Recorded Presence w/5m buffer
▢ Pond
▢ Predicted Abensce
▢ Predicted Presence

Figure 14: Graphs that represent the total frequency of both *H. maculata* presence points and their probabilities of predicting presence, and pseudo-random generated absent points and their probabilities of predicting presence in the West plot. Values were extracted from the orthomosaic generated in Figure 10 with ArcGIS.
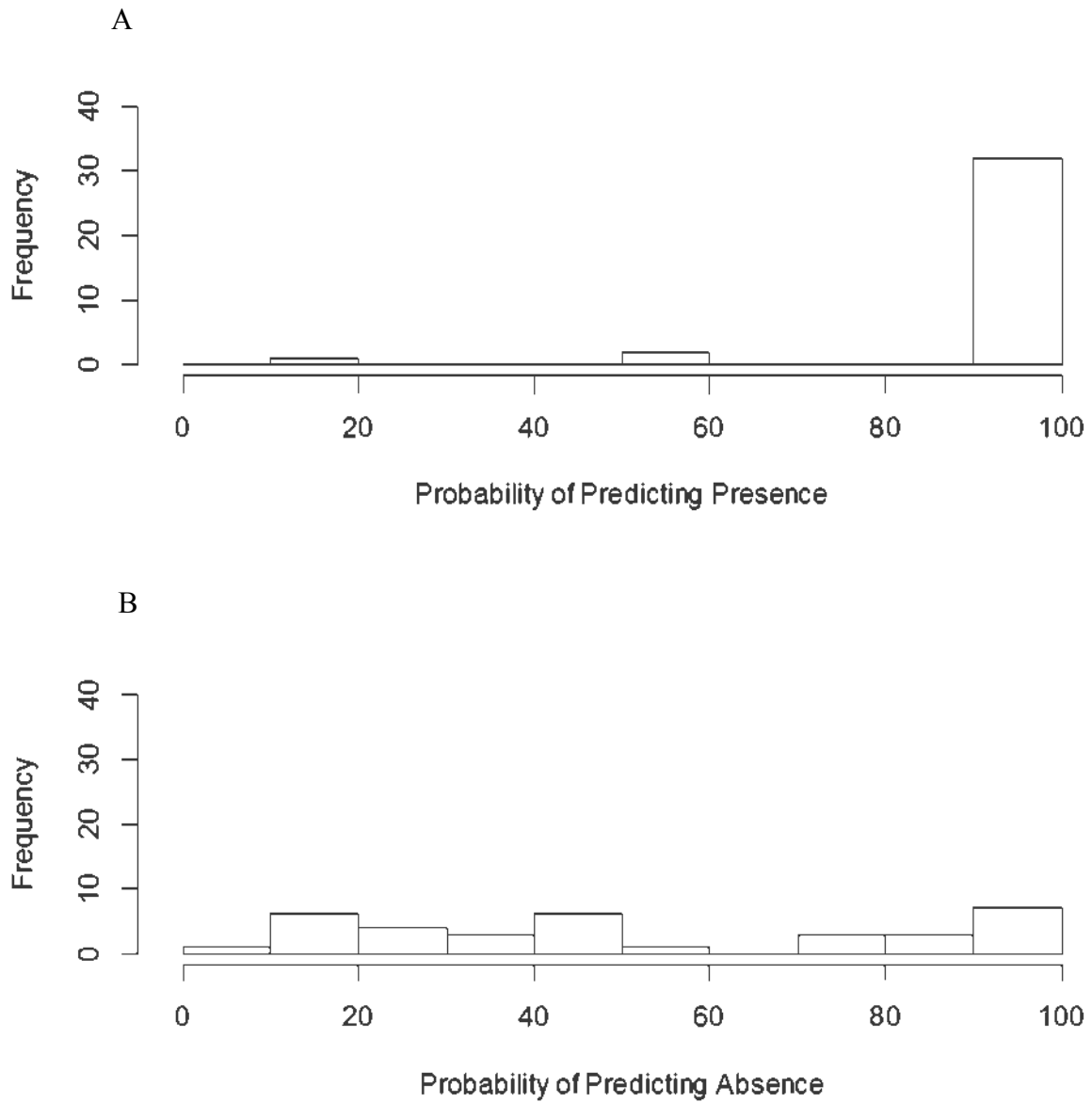
A

B

Figure 15: Graphs that represent the total frequency of both *H. maculata* presence points and their probabilities of predicting presence, and pseudo-random generated absent points and their probabilities of predicting presence in the South plot. Values were extracted from the orthomosaic generated in Figure 11 with ArcGIS.
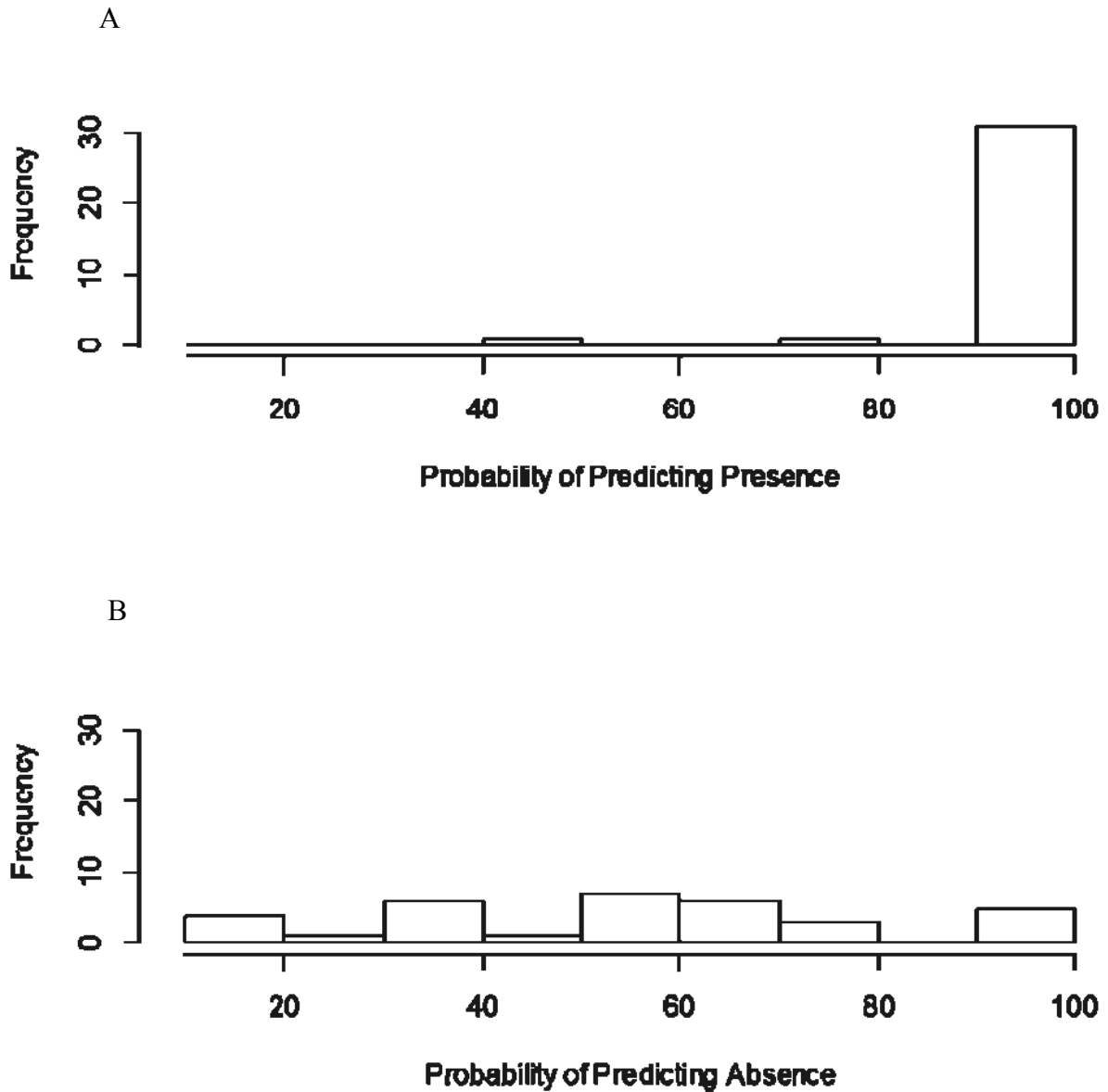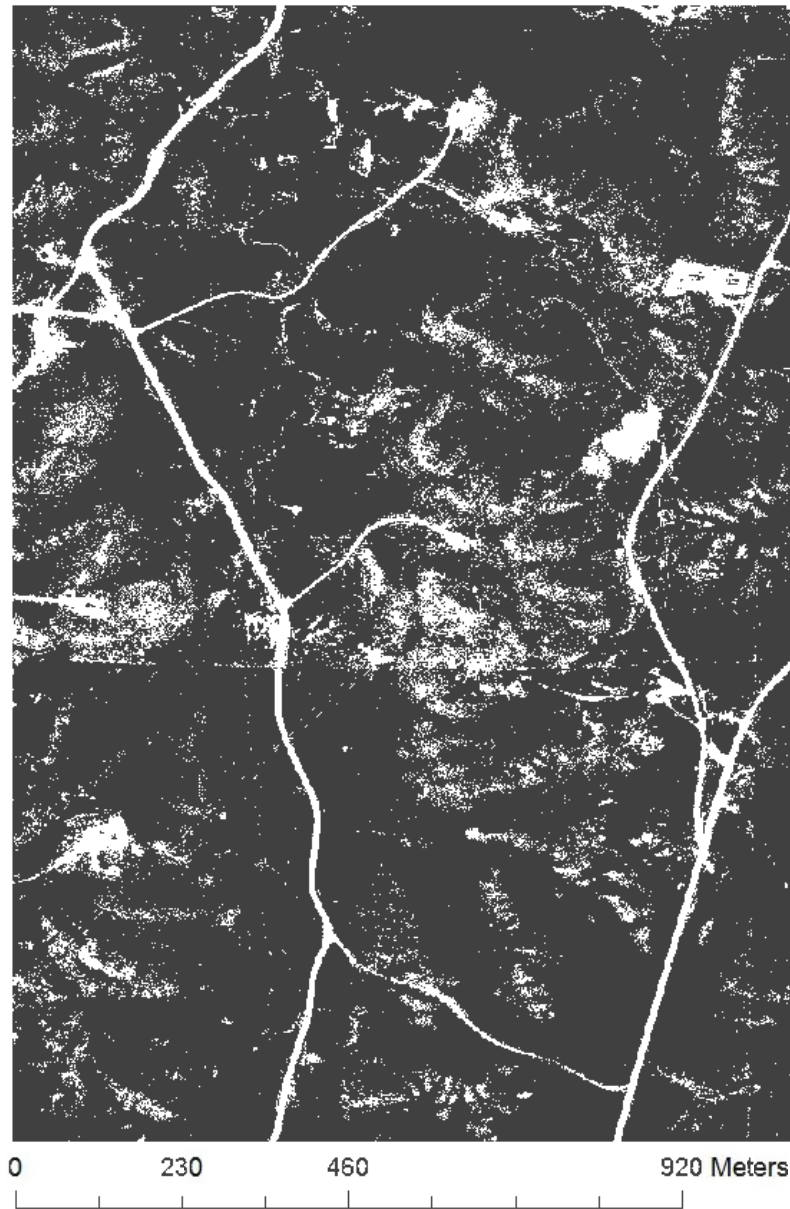
A

B

Figure 16: Orthomosaic of the Training plot generated in Agisoft Photoscan at Hadley Ranch and the Blue light (~470 nm) reflectance values. Images were captured in July, 2017.
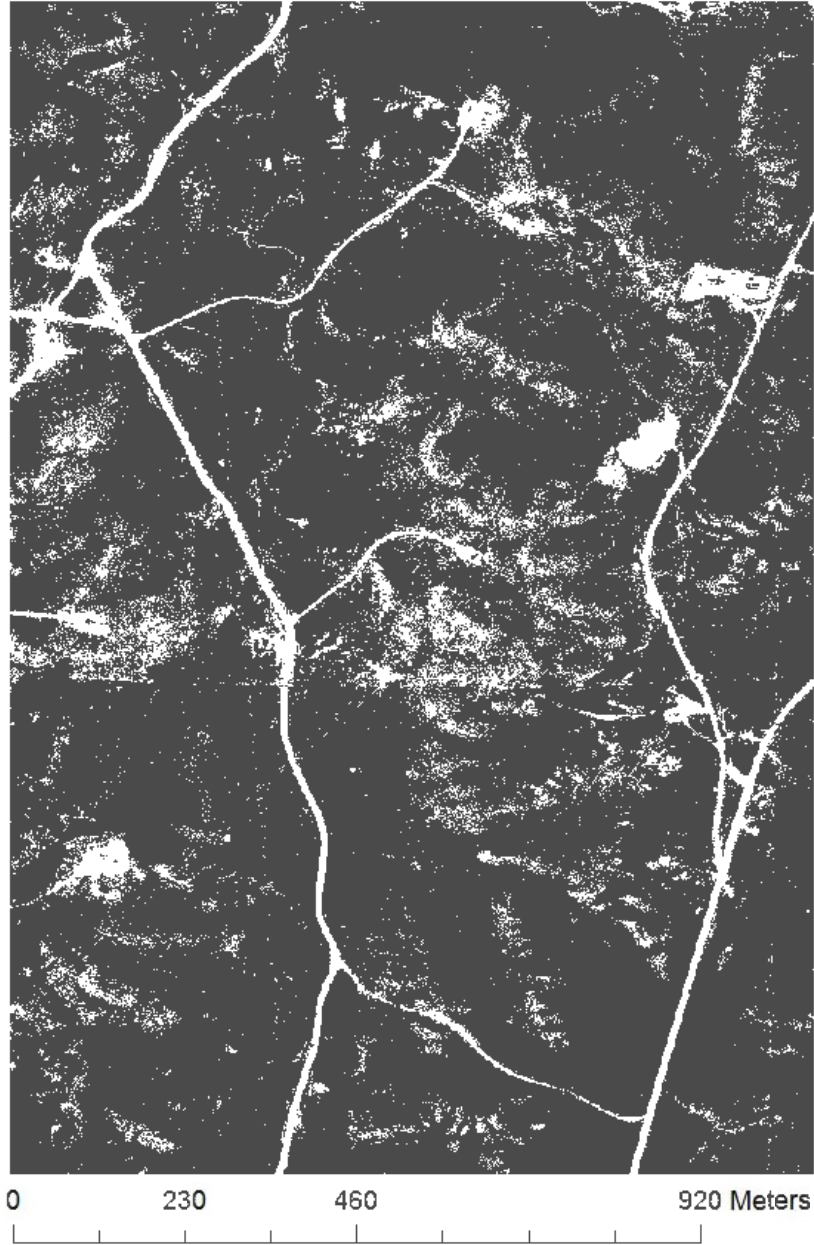

Blue Light Reflectance

Value
- High : 255

Low : 0

Figure 17: Orthomosaic of the Training plot generated in Agisoft Photoscan at Hadley Ranch and the Green light (~510 nm) reflectance values. Images captured in July, 2017.

Green Light Reflectance

Value

- High : 254

- Low : 0

Figure 18: Orthomosaic of the Training plot generated in Agisoft Photoscan at Hadley Ranch and the Near-infrared light (~710 nm) reflectance values. Images were captured in July, 2017.